Journal of Computational and Applied Mathematics 472 (2026) 116801

Contents lists available at ScienceDirect

Journal of Computational and Applied Mathematics

journal homepage: www.elsevier.com/locate/cam

Statistical testing-based framework for differentiating anomalous diffusion models with constant and random parameters

Katarzyna Maraj-Zygmąt [a,*], Aleksandra Grzesiek [a], Diego Krapf [b], Agnieszka Wyłomańska [a]

[a] Faculty of Pure and Applied Mathematics, Hugo Steinhaus Center, Wroclaw University of Science and Technology, 50-370 Wroclaw, Poland
[b] Department of Electrical and Computer Engineering and School of Biomedical Engineering, Colorado State University, Fort Collins, CO 80523, USA

ARTICLE INFO

Keywords:
Anomalous diffusion
Fractional Brownian Motion
Scaled Brownian motion
Statistical testing
Monte Carlo simulations
Real data analysis

ABSTRACT

Anomalous diffusion describes processes where the mean squared displacement scales non-linearly with time, $\mathbb{E}(X^2(t)) \sim t^\beta$, where β is termed the anomalous exponent. This behavior, seen in complex systems like biological cells, often defies standard diffusion models. Classical models such as fractional Brownian motion (FBM) and scaled Brownian motion (SBM) assume constant exponents, failing to capture dynamics with varying anomalous parameters. To address this limitations, models like FBM with random exponents (FBMRE) and SBM with random exponents (SBMRE) were introduced. This work proposes an universal procedure based on statistical testing framework that distinguishes between anomalous diffusion models with constant and random anomalous exponents using time-averaged statistics and their ratio-based counterparts. A novel procedure for optimizing time lag selection via divergence measure (here the Hellinger distance) is also proposed. The introduced methodology applies broadly to constant vs. random anomalous diffusion scenarios, with effectiveness depending on statistic selection, time lags, and process properties, as shown in simulations (with the two-point distribution of anomalous exponent) and real-world data analysis.

1. Introduction

Diffusion is a fundamental transport mechanism essential for the evolution of systems toward equilibrium. It describes the process by which particles migrate from regions of high concentration to regions of low concentration. This mechanism plays important roles across various disciplines, including biology, physics, environmental science, and geology; see [1–5]. The classical description of diffusion, called normal diffusion – studied by Einstein [6] and Smoluchowski [7] – is characterized by a linear relation between the mean square displacement of particles and time. For the process $\{X(t)\}$, it is mathematically described as $\mathbb{E}(X^2(t)) \sim t$. However, in many complex systems, deviations from this linear behavior are observed, leading to so-called anomalous diffusion [8–13]. This type of diffusion is characterized by a power-law scaling of the mean squared displacement in time, that is, $\mathbb{E}(X^2(t)) \sim t^\beta$, where β is called the anomalous exponent or the anomalous diffusion parameter. When $\beta > 1$, indicating faster-than-normal motion at large time points, the process is referred to as superdiffusion. Conversely, when $\beta < 1$, reflecting slower motion at large time points, the process is named as subdiffusion.

There are several mathematical models that describe stochastic processes exhibiting anomalous diffusion. Two widely studied models can be seen as the generalizations of the classical Brownian motion: fractional Brownian motion (FBM) and scaled Brownian

* Corresponding author.
E-mail address: katarzyna.maraj-zygmat@pwr.edu.pl (K. Maraj-Zygmąt).

https://doi.org/10.1016/j.cam.2025.116801
Received 19 December 2024; Received in revised form 25 March 2025
Available online 5 June 2025

motion (SBM). FBM introduces the short- or long-time correlation by allowing dependent increments - the displacement at a given time depends on past increments. FBM is characterized by a Hurst exponent $0 < H < 1$, which controls the degree of correlation: for $H < 0.5$, the process shows subdiffusive behavior, and for $H > 0.5$, it exhibits superdiffusion, [14–16]. The memory effect of FBM leads to the above-mentioned anomalous diffusion with the anomalous exponent equal to $2H$. SBM, on the other hand, modifies the classical Brownian motion by directly scaling the time by an exponent $\alpha > 0$, [17,18]. Unlike FBM, SBM does not involve dependence between increments. Although the mentioned stochastic models may have different properties, leading to various forms of anomalous diffusion (such as FBM accounting for memory through dependent increments, or SBM introducing time scaling without memory effects), they share the characteristic of a power-law scaling of the second moment in time, which is a key feature for this type of models.

In the literature, various statistical methods have been explored to identify and characterize different types of diffusion behaviors. Specifically, researchers focus on statistics that capture unique properties of anomalous diffusion, such as the sample autocovariance function (ACVF) [16,19–21], time average mean-squared displacement (TAMSD) [22–24], empirical anomaly measure (EAM) [25], detrended moving average (DMA) [26]. The above-mentioned statistics can be represented in quadratic form, which allows for the identification of the underlying probability distributions and their key probabilistic properties, particularly in the case of Gaussian processes [27]. Apart from the mentioned techniques, there are also other methods used for anomalous diffusion analysis, such as power spectral density (PSD) [28]. All mentioned statistics are effective in analyzing anomalous diffusion, as they are sensitive to the non-linear scaling of the mean square displacement over time. This feature makes them widely applied in numerous studies for anomalous exponent estimation and statistical testing for anomalous diffusion models, e.g. [25,26,29–31]. The mentioned statistics were also used as the basis for machine learning techniques applied in the analysis of anomalous diffusion phenomenon, [32,33].

However, recent studies highlight that classical anomalous diffusion models may be inadequate for certain complex systems. For example, one may mention the dynamics within the biological cell – often exhibiting anomalous diffusion – since in numerous studies the research indicates that the exponent is randomly evaluated across different trajectories [34–37]. One way to address this phenomenon is to generalize the classical anomalous models by introducing randomness in the anomalous exponents. For FBM, in [38] the constant H is replaced by a random variable defined on the interval $(0, 1)$, introducing the so-called fractional Brownian motion with random Hurst exponent (FBMRE). In [39] the authors analyze the basic properties of the scaled Brownian motion with random parameter (SBMRE).

The problem of distinguishing between models with constant and random anomalous exponents was considered in [40], where the authors discussed FBM versus FBMRE suggesting EAM statistics-based approach. In this paper, we build on these results by presenting a general method that can be applied to such problems. The procedure is demonstrated for FBM versus FBMRE and SBM vs SBMRE scenarios and relies on the TAMSD, EAM, and DMA statistics. Alongside classical statistics we also analyze their ratio counterparts, which have been suggested in the literature as alternatives to address issues arising from constant diffusion terms in theoretical formulas [41]. The procedure we propose requires determining optimal time lags, which may vary depending on the process and the statistics used. To identify these optimal values, we introduce a method based on analyzing the distances between the distributions of processes with constant and random coefficients, using Hellinger divergence measure as a guiding principle for optimization [42,43]. In the simulation study, as an example, we limit the analysis of FBMRE and SBMRE to the case of a two-point distribution of the anomalous exponent. Our method is easy adaptable: it can be used with any time-averaged statistics and may address any scenario involving constant versus random anomalous diffusion by following the steps proposed here. However, as we emphasize in the paper, the effectiveness of the proposed approach depends on the choice of statistics, the time lags used for these statistics, and the key properties of the underlying process.

The simulation results are supported by real data analysis. We consider two datasets coming from different areas. The first dataset corresponds to the motion of individual polystyrene microspheres in agarose hydrogels. This motion has previously been characterized as FBM [31,44]. However, here the results on FBMRE give new light for the analysis. These results exemplify a simple system in which it is important to understand the homogeneity (or lack thereof) of the environment and of the particles from a technological perspective. The second dataset represents the daily closing prices of Bitcoin and was discussed in the literature [40,45], where FBM was proposed as an appropriate model. The methodology proposed in this paper clearly supports this conclusion.

The remainder of the paper is organized as follows. Section 2 introduces two classical models of anomalous diffusion, FBM and SBM, along with their counterparts FBMRE and SBMRE. Section 3 presents the selected time-averaged statistics used to differentiate processes with random and constant anomalous exponents, along with their properties. Section 4 outlines the methodology for distinguishing processes and proposes a method for identifying the optimal time lags for the used statistics to ensure maximum classification efficiency. Section 5 provides simulation results. Section 6 showcases the analysis of real-world datasets. Section 7 concludes with a summary of findings and final remarks.

2. Anomalous diffusion models with constant and random anomalous exponents

In this part, we present definitions and selected properties of the processes that will be discussed in the subsequent sections. Our focus is on two classical processes that describe anomalous diffusion: fractional Brownian motion and scaled Brownian motion, along with their counterparts featuring random anomalous exponents. Please note that the definitions and properties presented in this section are well-established in the literature. As the classical reference on FBM, we refer readers to [46], where the process was introduced, and for SBM, to [47]. For the randomly anomalous exponents counterparts, we refer to [38] for FBMRE and [39] for SBMRE, where these processes are presented and described in detail.

2.1. Fractional Brownian motion

Fractional Brownian motion (FBM) $\{X_H(t), t \geq 0\}$ is a continuous centered Gaussian process defined as follows

$$X_H(t) = \sqrt{2D}\left[\int_0^t (t-u)^{H-1/2} d\tilde{B}(u) + \int_{-\infty}^0 \left((t-u)^{H-1/2} - (-u)^{H-1/2} d\tilde{B}(u)\right)\right], \tag{1}$$

see e.g. [46,48], where $0 < H < 1$ is the Hurst exponent and $\{\tilde{B}(t), t \in \mathbb{R}\}$ is the extension of the Brownian motion (BM) to the negative time axis. Namely, the process $\{\tilde{B}(t), t \in \mathbb{R}\}$ is defined as

$$\tilde{B}(t) = \begin{cases} B_1(t) & \text{for } t > 0 \\ B_2(-t) & \text{for } t \leq 0, \end{cases} \tag{2}$$

where $\{B_1(t), t \geq 0\}$ and $\{B_2(t), t \geq 0\}$ are two independent Brownian motions. The diffusion coefficient $D > 0$ is chosen in such way that for any $t \geq 0$, $\{X_H(t)\}$ is a continuous and zero-mean Gaussian process with variance equal to $\mathbb{E}(X_H^2(t)) = t^{2H}$, see for instance [29]. FBM is a self-similar process with stationary increments, zero mean, and autocovariance function (ACVF) given by the following formula

$$\text{ACVF}(X_H(t), X_H(s)) = \mathbb{E}[X_H(t)X_H(s)] = \frac{1}{2}(t^{2H} + s^{2H} - |t-s|^{2H}), \tag{3}$$

where $t, s \geq 0$. For a given $t \geq 0$ the random variable $X_H(t)$ is normally distributed with zero mean and variance equal to t^{2H}.

It is worth noting that for $H = 1/2$, FBM becomes classical Brownian motion. In contrast, for $H < 1/2$, the process exhibits subdiffusive behavior with negatively correlated increments, while for $H > 1/2$, it demonstrates superdiffusive behavior with positively correlated increments.

2.2. Fractional Brownian motion with random hurst exponent

The fractional Brownian motion with a random Hurst exponent $\{X_{\mathcal{H}}(t), t \geq 0\}$ is a process defined as a generalization of FBM described in the previous section. This is formulated by replacing the constant Hurst exponent H in the integral representation given in Eq. (1) with a random variable $\mathcal{H}$ [38]. The random variable $\mathcal{H}$ is defined on the interval $(0, 1)$, with the probability density function (PDF) $f_{\mathcal{H}}(h)$, and it is assumed to be independent of the process $\{\tilde{B}(t)\}$. The increments of FBMRE are stationary, and the PDF of $X_{\mathcal{H}}(t)$ for a given $t > 0$ is given by [38]

$$f_{X_{\mathcal{H}}(t)}(x) = \int_0^1 \frac{1}{\sqrt{2\pi t^{2h}}} \exp\left\{\frac{-x^2}{2t^{2h}}\right\} f_{\mathcal{H}}(h)dh \tag{4}$$

for $x \in \mathbb{R}$. Moreover, the autocovariance function of FBMRE is as follows [38]

$$\text{ACVF}(X_{\mathcal{H}}(t), X_{\mathcal{H}}(s)) = \mathbb{E}[X_{\mathcal{H}}(t)X_{\mathcal{H}}(s)] = \frac{1}{2}\left(M_{\mathcal{H}}(2\log(t)) + M_{\mathcal{H}}(2\log(s)) - M_{\mathcal{H}}(2\log(|t-s|))\right) \tag{5}$$

for $t, s \geq 0$, where $M_{\mathcal{H}}(x) = \mathbb{E}(\exp\{\mathcal{H}x\})$ denotes the moment generating function of the random variable $\mathcal{H}$.

In this paper, we focus on a specific example of the distribution of the Hurst exponent $\mathcal{H}$, namely the two-point ($\mathcal{TP}$) distribution. As recalled from [40], the two-point distribution is concentrated at points $0 < H_1 < H_2 < 1$, with probability masses p and $1-p$ (where $p \in [0, 1]$). The PDF of this distribution is given by

$$f_{\mathcal{H}}(h) = p\delta(h - H_1) + (1-p)\delta(h - H_2), \tag{6}$$

where $\delta(\cdot)$ is the Dirac delta function. We denote this distribution as $\mathcal{TP}(H_1, H_2, p)$.

2.3. Scaled Brownian motion

The scaled Brownian motion $\{B_\alpha(t), t \geq 0\}$ is a continuous centered Gaussian process defined as follows [47]

$$B_\alpha(t) = B(t^\alpha), \tag{7}$$

where $\{B(t)\}$ is the standard Brownian motion, and $\alpha > 0$ is the anomalous exponent. SBM is a zero-mean self-similar process, and its autocovariance function is defined as

$$\text{ACVF}(B_\alpha(s), B_\alpha(t)) = \mathbb{E}[B_\alpha(t)B_\alpha(s)] = \min\{t^\alpha, s^\alpha\} \tag{8}$$

for $t, s \geq 0$. For a given $t \geq 0$, the random variable $B_\alpha(t)$ is Gaussian distributed with zero mean and variance equal to t^α. It is worth noting that the increments of SBM are independent, similar to those of Brownian motion. Although the general definition assumes $\alpha > 0$, in our work, we constrain the parameter α by assuming $\alpha \in (0, 2)$. This restriction allows for a comparison of results in the FBM case.

The SBM process is considered a generalization of Brownian motion, since, for $\alpha = 1$, SBM becomes equivalent to BM. When $\alpha < 1$, the process is subdiffusive, whereas for $\alpha > 1$, it exhibits superdiffusive behavior. For further information regarding this process, we refer to [49–52].

2.4. Scaled Brownian motion with random anomalous exponent

The scaled Brownian motion with random anomalous diffusion $\{B_{\mathcal{A}}(t)\}$ is defined as a generalization of the scaled Brownian motion described in the previous subsection. Similarly to how FBMRE arises from FBM, SBMRE is formulated by replacing the parameter α in Eq. (7) with a random variable $\mathcal{A}$. Here, $\mathcal{A}$ is a positive random variable that takes values from the interval $(0, 2)$ and it is assumed to be independent of the process $\{B(t)\}$ [39]. The SBMRE process has independent increments, and the PDF of $B_{\mathcal{A}}(t)$ for a given $t > 0$ has the following form

$$f_{B_{\mathcal{A}}(t)}(x) = \int_0^2 \frac{1}{\sqrt{2\pi t^{\alpha}}} \exp\left\{\frac{-x^2}{2t^{\alpha}}\right\} f_{\mathcal{A}}(\alpha) d\alpha \tag{9}$$

for $x \in \mathbb{R}$. The ACVF of SBMRE is given by the following formula

$$\mathrm{ACVF}(B_{\mathcal{A}}(s), B_{\mathcal{A}}(t)) = \mathbb{E}[B_{\mathcal{A}}(t)B_{\mathcal{A}}(s)] = M_{\mathcal{A}}(\log(\min\{t, s\})) \tag{10}$$

for $t, s \geq 0$, where $M_{\mathcal{A}}(\cdot)$ denotes the moment-generating function of the random variable $\mathcal{A}$.

In the following sections, similar to the FBMRE case, we assume that $\mathcal{A}$ is a random variable from the two-point distribution $\mathcal{TP}(\alpha_1, \alpha_2, p)$. In this case, the distribution is concentrated at points $0 < \alpha_1 < \alpha_2 < 2$, with probability masses p and $1 - p$ (where $p \in [0, 1]$), i.e., with the following PDF

$$f_{\mathcal{A}}(h) = p\delta(h - \alpha_1) + (1 - p)\delta(h - \alpha_2), \tag{11}$$

where $\delta(\cdot)$ is the Dirac delta function.

3. Time-averaged statistics

In this section, we review the definitions of three statistics that can be used to differentiate between processes with random and constant anomalous diffusion parameters: the time-averaged mean squared displacement, empirical anomaly measure, and detrended moving average statistic. In the following discussion, let us denote a sample trajectory of length n of a stochastic process $\{X(t)\}$ as $\mathbb{X}_n = \{X(1), X(2), \ldots, X(n)\}$.

3.1. Time-averaged mean squared displacement

For the trajectory $\mathbb{X}_n$, the time-averaged mean squared displacement statistic is defined as follows

$$\mathrm{TAMSD}(\mathbb{X}_n, \tau) = \frac{1}{n - \tau} \sum_{i=1}^{n-\tau} (X(i + \tau) - X(i))^2, \tag{12}$$

for any time lag $\tau = 1, 2, \ldots, n - 1$. For the finite trajectory of a zero-mean stochastic process the statistic given in Eq. (12) can be expressed using the so-called quadratic form representation via the following formula

$$\mathrm{TAMSD}(\mathbb{X}_n, \tau) = \frac{1}{2}\mathbb{X}_n \mathbb{A}(\tau) \mathbb{X}_n^T, \tag{13}$$

where the symbol V^T denotes vector transposition of the vector V, and $\mathbb{A}(\tau)$ is the $n \times n$ tridiagonal symmetric matrix $\mathbb{A}(\tau) = \{a(\tau; i, j)\}_{i,j=1}^{n}$. The elements of matrix $\mathbb{A}(\tau)$ are given by the expression

$$a(\tau; i, j) = \frac{2}{n - \tau}\left(m_i \mathbb{I}(i = j) - \mathbb{I}(|i - j| = \tau)\right), \tag{14}$$

where

$$m_i = \begin{cases} \begin{cases} 1, i \leq \tau \text{ or } i \geq n - \tau \\ 2, \tau < i < n - \tau, \end{cases} & \tau \leq n/2, \\ \begin{cases} 1, i \geq \tau \text{ or } i \leq n - \tau \\ 0, n - \tau < i < \tau, \end{cases} & \tau > n/2 \end{cases}$$

and $\mathbb{I}(x \in B)$ is the indicator function that is equal to 1 if $x \in B$ and 0 otherwise. As a result of the representation given in Eq. (13), the distribution of TAMSD for FBM and other general Gaussian processes is well-established and thoroughly discussed, according to the theory of quadratic forms for Gaussian processes [53]. We also note that TAMSD is one of the most classical statistics used in the characterization of anomalous diffusion, see for instance [54–57]. Below, we provide the formulas for expected values of TAMSD for all processes considered in this paper. Please note that the results presented in Fact 1 are well-established in the literature, as TAMSD has been previously studied for the considered processes. The relevant references are provided within the statement.

Fact 1.

1. *Let $\mathbb{X}_n$ denote a trajectory of FBM process defined in Eq. (1), then the expected value for TAMSD is given by the following formula [55]*

$$\mathbb{E}(\mathrm{TAMSD}(\mathbb{X}_n, \tau)) = \tau^{2H}. \tag{15}$$

2. *Let $\mathbb{X}_n$ denote a trajectory of SBM process defined in Eq. (7), then the expected value for TAMSD is given by the following formula [58]*

$$\mathbb{E}(\mathrm{TAMSD}(\mathbb{X}_n,\tau)) = \frac{n^{\alpha+1} - \tau^{\alpha+1} - (n-\tau)^{\alpha+1}}{(\alpha+1)(n-\tau)}. \tag{16}$$

3. *Let $\mathbb{X}_n$ denote a trajectory of FBMRE process defined in Section 2.2, then the expected value for TAMSD is given by the following formula [38]*

$$\mathbb{E}(\mathrm{TAMSD}(\mathbb{X}_n,\tau)) = \mathrm{M}_{\mathcal{H}}(2\log(\tau)), \tag{17}$$

where $\mathrm{M}_{\mathcal{H}}(\cdot)$ denotes the moment generating function of the random Hurst exponent $\mathcal{H}$.

4. *Let $\mathbb{X}_n$ denote a trajectory of SBMRE process defined in Section 2.4, then the expected value for TAMSD is given by the following formula [39]*

$$\mathbb{E}(\mathrm{TAMSD}(\mathbb{X}_n,\tau)) = \frac{1}{n-\tau}\sum_{i=1}^{n-\tau}(\mathrm{M}_{\mathcal{A}}(\log(i+\tau)) - \mathrm{M}_{\mathcal{A}}(\log(i))), \tag{18}$$

where $\mathrm{M}_{\mathcal{A}}(\cdot)$ denotes the moment generating function of the random scaling parameter $\mathcal{A}$.

In Appendix A, we present the formulas for the expected values of TAMSD for FBMRE and SBMRE with two-point distributed anomalous exponents, see Fact 4, which are determined based on Eqs. (17) and (18) and follow from the form of the moment generating function.

3.2. Empirical anomaly measure

For the trajectory $\mathbb{X}_n$ the empirical anomaly measure, introduced in [25], is given by the following formula

$$\mathrm{EAM}(\mathbb{X}_n,\tau) = 2\sum_{i=1}^{\tau-1}(\tau-i)\hat{\gamma}_{\mathbb{Y}}(i), \tag{19}$$

for any time lag $\tau = 1,2,\dots,n-1$. In above equation $\hat{\gamma}_{\mathbb{Y}}(i)$ is the empirical ACVF of the increments' process denoted as $\mathbb{Y}_{n-1} = \{Y(1),Y(2),\dots,Y(n-1)\}$, where $Y(j) = X(j+1) - X(j)$ for $j = 1,2,\dots,n-1$, given as follows

$$\hat{\gamma}_{\mathbb{Y}}(i) = \frac{1}{n-1}\sum_{j=1}^{n-i} Y(j)Y(j+1), \quad i = 1,2,\dots,n-1. \tag{20}$$

For the finite trajectory $\mathbb{X}_n$ of the zero-mean stochastic process with stationary increments, the EAM can be represented as the quadratic form of the increments' vector $\mathbb{Y}_{n-1}$, namely

$$\mathrm{EAM}(\mathbb{X}_n,\tau) = \mathbb{Y}_{n-1}^{\mathsf{T}}\mathbb{T}(\tau)\mathbb{Y}_{n-1}, \tag{21}$$

where $\mathbb{T}(\tau) = \left[t_{|i-j|}\right]$, $i,j = 1,2,\dots,n-1$ is the indefinite symmetric Toeplitz matrix of the bandwidth $\tau-1$ ($\tau > 1$) with $t_{|i-j|} = \frac{\tau-|i-j|}{n-1-|i-j|}\mathbb{I}(0 < |i-j| < \tau)$.

As mentioned, the EAM was introduced in [25], where it was discussed as an estimator of the anomaly measure (AM). The quantity called AM for the process $\{X(t)\}$ of stationary increments is defined as follows

$$AM(\tau) = 2\sum_{i=1}^{\tau-1}(\tau-i)\hat{\gamma}_Y(i), \tag{22}$$

where $\{Y(t)\}$ is the increment process of $\{X(t)\}$ and γ_Y is its ACVF. In addition, we have [25]

$$\mathbb{E}(X^2(\tau)) = \tau\gamma_Y(0) + 2\sum_{i=1}^{\tau-1}(\tau-i)\gamma_Y(i). \tag{23}$$

Thus, the quantity given in Eq. (23) can be represented as

$$AM(\tau) = \mathbb{E}(X^2(\tau)) - \tau\gamma_Y(0). \tag{24}$$

Therefore, the AM provides information about the deviation of $\mathbb{E}[X^2(\tau)]$ from the linear function of time $\tau\gamma_Y(0)$. Thus, AM is a measure that assesses the anomalous diffusive behavior of the process $\{X(t)\}$, and its estimator, the EAM, can be considered a natural statistic for this assessment. More details about the physical interpretation of the EAM are discussed in [25].

Given the quadratic form representation, the probabilistic properties of EAM for Gaussian processes are studied in [31]. Below, we provide the formulas for expected values of EAM for FBM and FBMRE processes. Please note that the results given in Fact 2 are well-known in the literature, with the relevant references included in the statement. Let us emphasize that, since the increments of

SBM and SBMRE are independent, we omit the presentation of the EAM in these cases, as it relies on the ACVF of the increments, which is zero for all $\tau \geq 1$.

Fact 2.

1. *Let $\mathbb{X}_n$ denote a trajectory of FBM process defined in Eq. (1), then the expected value for EAM is given by the following formula [25]*

$$\mathbb{E}(\mathrm{EAM}(\mathbb{X}_n, \tau)) = \tau^{2H} - \tau. \tag{25}$$

2. *Let $\mathbb{X}_n$ denote a trajectory of FBMRE process defined in Section 2.2, then the expected value for EAM is given by the following formula [40]*

$$\mathbb{E}(\mathrm{EAM}(\mathbb{X}_n, \tau)) = \mathrm{M}_{\mathcal{H}}(2\log(\tau)) - \tau, \tag{26}$$

where $\mathrm{M}_{\mathcal{H}}(\cdot)$ denotes the moment generating function of the random Hurst exponent $\mathcal{H}$.

In Appendix A, we present the formula for the expected values of EAM for FBMRE with two-point distributed anomalous exponents, see Fact 5, which is determined based on Eq. (26) and follows from the form of the moment generating function.

3.3. Detrended moving average statistic

For the trajectory $\mathbb{X}_n$ the detrended moving average statistic established in [59] is defined as follows

$$\mathrm{DMA}(\tau) = \frac{1}{n-\tau}\sum_{j=\tau}^{n}\left(X(j) - \bar{X}^{\tau}(j)\right)^2, \tag{27}$$

for any time lag $\tau = 2, 3, \ldots, n-1$. In Eq. (27) the symbol $\bar{X}^{\tau}(j)$ denotes a moving average of τ observations $X(j), \ldots, X(j-\tau+1)$, i.e.,

$$\bar{X}^{\tau}(j) = \frac{1}{\tau}\sum_{i=0}^{\tau-1} X(j-i). \tag{28}$$

As shown in [26], the DMA statistic has a quadratic form representation not in terms of original sample trajectory $\mathbb{X}_n$ but in terms of the detrended process denoted as $\mathbb{Z}_n = (Z(1), \ldots, Z(n-\tau+1))$, where $Z(i) = X(i+\tau-1) - \hat{X}^{\tau}(i+\tau-1)$. The mentioned representation is as follows

$$\mathrm{DMA}(\tau) = \frac{1}{N-\tau}\mathbb{Z}_n\mathbb{Z}_n^T. \tag{29}$$

Let us notice that the statistic $\mathrm{DMA}(\tau)$ is a random quantity that measures the mean squared distance between the original process $X(j)$ and its moving average $\bar{X}^{\tau}(j)$ over the window of size τ. Its probabilistic properties are studied in [26], where FBM is discussed in detail. Below, based on those results, we provide the formulas for expected values of DMA for all processes considered in this paper and, to the best of our knowledge, the formulas for expected values of DMA in case of FBMRE, SBM, and SBMRE have not been previously presented.

Fact 3.

1. *Let $\mathbb{X}_n$ denote a trajectory of FBM process defined in Eq. (1), then the expected value for DMA is given by the following formula [26]*

$$\begin{aligned}\mathbb{E}(\mathrm{DMA}(\mathbb{X}_n, \tau)) = &\frac{1}{n-\tau}\sum_{j=\tau}^{n}\left\{\left(1-\frac{1}{\tau}\right)^2 j^{2H} + \left(\frac{1}{\tau^2}-\frac{1}{\tau}\right)\sum_{m=j-\tau+1}^{j-1}\left(j^{2H}+m^{2H}-|j-m|^{2H}\right)\right.\\ &\left.+\frac{1}{\tau^2}\sum_{m=j-\tau+1}^{j-1} m^{2H} + \frac{2}{\tau^2}\sum_{j-\tau+1\leq l<m\leq j-1}\left(m^{2H}+l^{2H}-|m-l|^{2H}\right)\right\}.\end{aligned} \tag{30}$$

2. *Let $\mathbb{X}_n$ denote a trajectory of SBM process defined in Eq. (7), then the expected value for DMA is given by the following formula*

$$\begin{aligned}\mathbb{E}(\mathrm{DMA}(\mathbb{X}_n, \tau)) = &\frac{1}{n-\tau}\sum_{j=\tau}^{n}\left\{\left(1-\frac{1}{\tau}\right)^2 j^{\alpha} + 2\left(\frac{1}{\tau^2}-\frac{1}{\tau}\right)\sum_{m=j-\tau+1}^{j-1}\min\{j^{\alpha}, m^{\alpha}\} + \frac{1}{\tau^2}\sum_{m=j-\tau+1}^{j-1} m^{\alpha}\right.\\ &\left.+\frac{2}{\tau^2}\sum_{j-\tau+1\leq l<m\leq j-1}\min\{m^{\alpha}, l^{\alpha}\}\right\}.\end{aligned} \tag{31}$$

3. *Let $\mathbb{X}_n$ denote a trajectory of FBMRE process defined in Section 2.2, then the expected value for DMA is given by the following formula*

$$\mathbb{E}(\mathrm{DMA}(\mathbb{X}_n,\tau)) = \frac{1}{n-\tau}\sum_{j=\tau}^{n}\Bigg\{\left(1-\frac{1}{\tau}\right)^2 \mathrm{M}_{\mathcal{H}}(2\log(j)) + \left(\frac{1}{\tau^2}-\frac{1}{\tau}\right)\sum_{m=j-\tau+1}^{j-1}\left(\mathrm{M}_{\mathcal{H}}(2\log(j))+\mathrm{M}_{\mathcal{H}}(2\log(m))-\mathrm{M}_{\mathcal{H}}(2\log(|j-m|))\right) + \frac{1}{\tau^2}\sum_{m=j-\tau+1}^{j-1}\mathrm{M}_{\mathcal{H}}(2\log(m)) + \frac{2}{\tau^2}\sum_{j-\tau+1\le l<m\le j-1}\left(\mathrm{M}_{\mathcal{H}}(2\log(m))+\mathrm{M}_{\mathcal{H}}(2\log(l))-\mathrm{M}_{\mathcal{H}}(2\log(|m-l|))\right)\Bigg\}. \tag{32}$$

where $\mathrm{M}_{\mathcal{H}}(\cdot)$ *denotes the moment generating function of the random Hurst exponent* $\mathcal{H}$.

4. *Let* $\mathbb{X}_n$ *denote a trajectory of SBMRE process defined in Section 2.4, then the expected value for DMA is given by the following formula*

$$\mathbb{E}(\mathrm{DMA}(\mathbb{X}_n,\tau)) = \frac{1}{n-\tau}\sum_{j=\tau}^{n}\Bigg\{\left(1-\frac{1}{\tau}\right)^2 \mathrm{M}_{\mathcal{A}}(\log(j)) + 2\left(\frac{1}{\tau^2}-\frac{1}{\tau}\right)\sum_{m=j-\tau+1}^{j-1}\mathrm{M}_{\mathcal{A}}(\log(\min\{j,m\})) + \frac{1}{\tau^2}\sum_{m=j-\tau+1}^{j-1}\mathrm{M}_{\mathcal{A}}(\log(m)) + \frac{2}{\tau^2}\sum_{j-\tau+1\le l<m\le j-1}\mathrm{M}_{\mathcal{A}}(\log(\min\{m,l\}))\Bigg\}. \tag{33}$$

where $\mathrm{M}_{\mathcal{A}}(\cdot)$ *denotes the moment generating function of the random scaling parameter* $\mathcal{A}$.

In Appendix A, we present the formulas for the expected values of DMA for FBMRE and SBMRE with two-point distributed anomalous exponents, see Fact 6, which are determined based on Eqs. (32) and (33) and follow from the form of the moment generating function of the two-point distribution.

In the literature, in addition to the statistics defined in the previous subsections, their relative versions are also considered, which are calculated as the ratios between these statistics for two different values of τ, i.e.,

$$\mathrm{TAMSD}_{\mathrm{R}}(\mathbb{X}_n,\vec{\tau}) = \frac{\mathrm{TAMSD}(\mathbb{X}_n,\tau_1)}{\mathrm{TAMSD}(\mathbb{X}_n,\tau_2)},\ \mathrm{EAM}_R(\mathbb{X}_n,\vec{\tau}) = \frac{\mathrm{EAM}(\mathbb{X}_n,\tau_1)}{\mathrm{EAM}(\mathbb{X}_n,\tau_2)}, \tag{34}$$

$$\text{and } \mathrm{DMA}_R(\mathbb{X}_n,\vec{\tau}) = \frac{DMA(\mathbb{X}_n,\tau_1)}{DMA(\mathbb{X}_n,\tau_2)}, \tag{35}$$

where $\vec{\tau} = (\tau_1,\tau_2)$ is a vector of time lags, see for instance [60,61]. In our analysis, we also apply ratio statistics to discriminate anomalous diffusive processes with constant and random parameters.

In Figs. 1 and 2, the empirical expected values of the aforementioned statistics are shown for all processes considered in the paper. In Fig. 1 we present results for classical statistics and in Fig. 2 results for ratio statistics are shown. To calculate expected values, we use $MC = 1000$ trajectories of length $N = 1000$. For each trajectory, we compute the value of the statistic for the selected τ values. For the classical statistics, we examine $\tau = 2,3,4,\dots,20$, while for the ratio statistics, we set $\tau_1 = 2$ and $\tau = \tau_2 = 3,4,\dots,20$. Then, for each τ, we calculate the sample mean based on the MC values of the respective statistics. In order to compare the results in both cases, i.e. for the classical and ratio statistics, we present the results starting from $\tau = 3$.

In Figs. 1(a) and 2(a), we present results for the FBM process with $H = 0.4$. Figs. 1(b) and 2(b) show results for FBMRE with $\mathcal{H} \sim \mathcal{TP}(0.2, 0.8, 2/3)$. In Figs. 1(c) and 2(c) explore the SBM process with $\alpha = 0.8$. Finally, Figs. 1(d) and 2(d) display results for SBMRE with $\mathcal{A} \sim \mathcal{TP}(0.4, 1.6, 2/3)$. The parameters of the two-point distributions for $\mathcal{H}$ and $\mathcal{A}$ are selected to ensure that their expected values are equal to H and α used in the FBM and SBM cases, respectively, i.e., $H = 0.4$ and $\alpha = 0.8$. For SBM, we do not present results for EAM and EAM_R because in this case, the EAM statistic is equal to zero (as this is a process of independent increments).

The primary observation from Figs. 1 and 2 is that the expected values of the ratio statistics are lower than those of the classical ones. All statistics have positive values, except the $\mathbb{E}(EAM)$ in the case of FBM. It is also notable that for processes with random parameters, expected values are higher than those for FBM and SBM, where the parameters are constant. For the classical statistics, the expected values for both statistics are increasing functions of τ. In contrast, for the ratio statistics, the larger the τ, the smaller the expected value. When we compare the expected values of the statistics for processes with constant versus random diffusion exponents, we observe that, while the mean values of the classical statistics differ significantly in the range of values or the shape of the graphs, these differences are much less noticeable for the ratio statistics. For example, the mean values for EAM_R in the cases of FBM and FBMRE are quite similar, which may suggest that ratio statistics are not very effective in distinguishing between these types of processes, contrary to the their classical versions.

4. Methodology for differentiating models with constant and random anomalous exponent

This section presents a step-by-step procedure for distinguishing between anomalous diffusion models with constant and random parameters. We apply this approach to differentiate between FBM and FBMRE in the first scenario and SBM and SBMRE in the second scenario. The algorithm outlined below is universal, applicable to all statistical measures discussed in this paper, and adaptable to both scenarios (FBM versus FBMRE and SBM versus SBMRE).

Let us assume that MC sample trajectories, each of length N, generated by the tested model are available. In our case, these trajectories correspond to FBM with a specified H_0 value or SBM with a specified parameter α_0. We denote these trajectories as

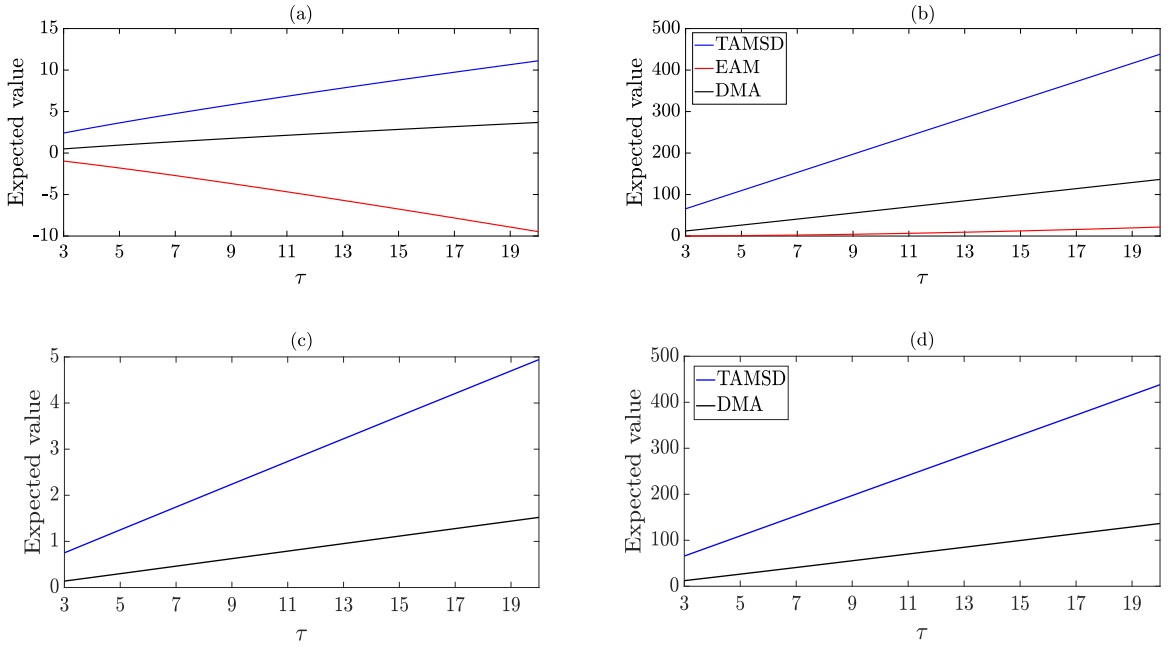

Fig. 1. Empirical expected values for TAMSD, EAM, and DMA calculated from 1000 trajectories of length $N = 1000$ of (a) FBM with $H = 0.4$, (b) FBMRE with $\mathcal{H} \sim \mathcal{TP}(0.2, 0.8, 2/3)$, (c) SBM with $\alpha = 0.4$, and (d) SBMRE with $\mathcal{A} \sim \mathcal{TP}(0.4, 1.6, 2/3)$. Expected values are calculated for $\tau = \{2, 3 \ldots, 20\}$.

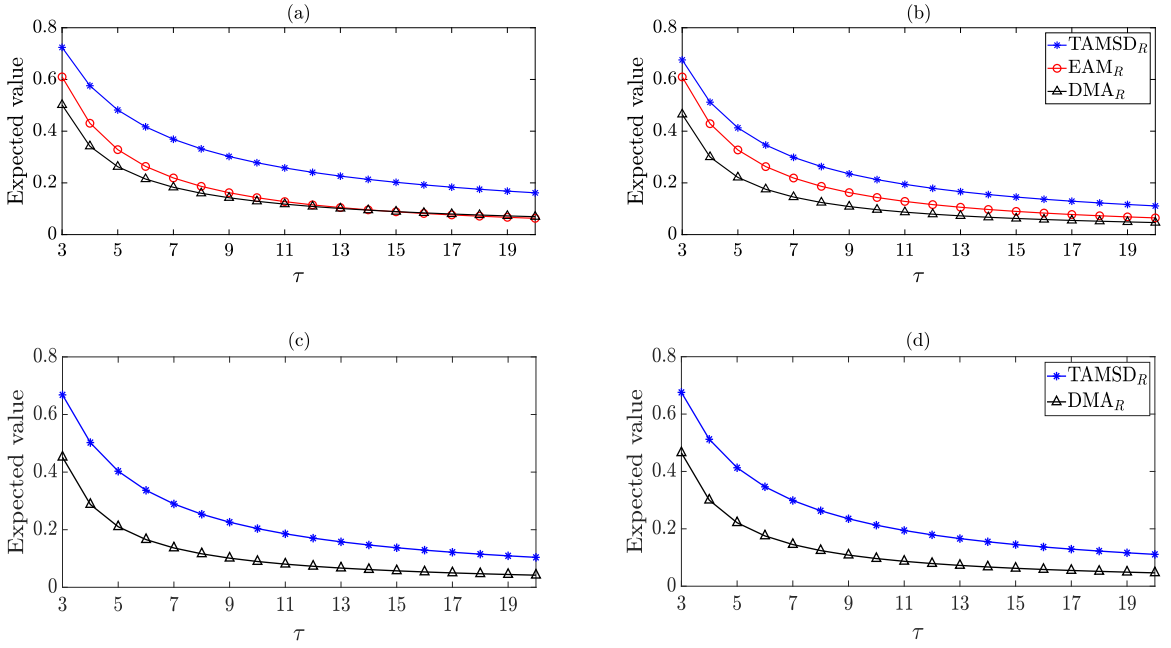

Fig. 2. Empirical expected values for TAMSD$_R$, EAM$_R$, and DMA$_R$ calculated from 1000 trajectories of length $N = 1000$ of (a) FBM with $H = 0.4$, (b) FBMRE with $\mathcal{H} \sim \mathcal{TP}(0.2, 0.8, 2/3)$, (c) SBM with $\alpha = 0.4$, and (d) SBMRE with $\mathcal{A} \sim \mathcal{TP}(0.4, 1.6, 2/3)$. Expected values are calculated for $\tau_1 = 2$ and $\tau = \tau_2 = \{3, 4, \ldots, 21\}$.

$\mathbb{X}_N^i$, where $i = 1, 2, \ldots, MC$. Here we assume that H_0 and α_0 are known, however, this methodology can easily be extended to the general case (i.e., when H_0 and α_0 are unknown). The differentiation procedure relies on hypothesis testing, with the null hypothesis asserting that the sample trajectory $\mathbb{X}_N^*$ originates from the anomalous diffusion model with constant parameter (in our case, either FBM or SBM). The algorithm is as follows:

- For a chosen τ calculate the test statistic for each sample trajectory $\mathbb{X}_N^i$, where $i = 1, 2, \ldots, MC$. Denote the resulting test statistic values as $D_1(\tau), D_2(\tau), \ldots, D_{MC}(\tau)$.

- Determine the acceptance region of the test of the following form

$$[Q_{c/2}(N,\tau), Q_{1-c/2}(N,\tau)], \tag{36}$$

where $Q_p(N,\tau)$ represents the quantile of order p of the test statistic's distribution under the null hypothesis. Since the theoretical distribution of the test statistic is unknown, calculate these quantiles empirically based on $D_1(\tau), D_2(\tau), \dots, D_{MC}(\tau)$.
- For a given trajectory $\mathbb{X}_N^*$, reject the null hypothesis if the test statistic $D^*(\tau)$, calculated for $\mathbb{X}_N^*$, falls outside the acceptance region given in Eq. (36); i.e., if the test statistic is extreme - either larger than the upper critical value or smaller than the lower critical value, at the specified significance level c. If the test statistic value $D^*(\tau)$ lies within the acceptance region there is no evidence to reject the null hypothesis.

In our analysis, the models under the alternative hypothesis – corresponding to the trajectory $\mathbb{X}_N^*$ – incorporate random parameters, i.e. we assume FBMRE in the first scenario and SBMRE in the second scenario. Furthermore, we assume that the random variables $\mathcal{H}$ (in the first scenario) and $\mathcal{A}$ (in the second scenario) follow a two-point distribution on the interval $(0,1)$ and $(0,2)$, respectively. Nevertheless, the procedure outlined above can also be applied to other types of distributions for anomalous exponents.

As mentioned, the presented procedure can be easily extended to the general case, allowing for no specific assumptions about the parameter values H_0 and α_0. In this case, we conduct the test for all possible values of H_0 and α_0 within the specified intervals and assess the number of null hypotheses corresponding to these values of the anomalous exponents. This approach is demonstrated in the real data analysis presented in Section 6.

4.1. Selection of optimal τ values

The key parameters in the methodology described above are the time lags, i.e., the τ value for classical statistics and the τ_1 and τ_2 values for ratio statistics. Therefore, in this section, we address the problem of selecting optimal time lag values. We propose a procedure that identifies values maximizing the separation between the distributions of the test statistics for FBM and FBMRE in the first scenario, and for SBM and SBMRE in the second scenario. We quantify the distributional difference using the Hellinger distance, a measure of divergence based on probability density functions [43]. While we illustrate the procedure using two-point distributions of anomalous exponents, it can also be applied to other types of distributions. The procedure is applicable to any of the statistics discussed in this paper; therefore, we present it in a general form, without specifying the particular statistic used. The steps are as follows:

1. Simulate MC trajectories of length N, denoted as $\mathbb{X}_N^i$, where $i = 1, 2, \dots, MC$, from FBM with given H_0 or for SBM with an assumed α_0.
2. For each trajectory from Step 1, calculate the value of the statistic for each specified τ values. For classical statistics take $\tau = 2, 3, \dots, 20$; for ratio statistics, evaluate all combinations of $\tau_1 = 2, 3, \dots, 20$ and $\tau_2 = 2, 3, \dots, 20$.
3. Simulate MC^* trajectories, denoted as $\mathbb{X}_N^{i*}$, where $i = 1, 2, \dots, MC^*$, from FBMRE with $\mathcal{H} \sim \mathcal{TP}(H_1, H_2, p)$ or SBMRE with $\mathcal{A} \sim \mathcal{TP}(\alpha_1, \alpha_2, p)$. The parameters of $\mathcal{H}$ and $\mathcal{A}$ distributions are chosen such that $\mathbb{E}(\mathcal{H}) = H_0$ and $\mathbb{E}(\mathcal{A}) = \alpha_0$. To simplify the analysis, we assume specific values for H_1, H_2 and α_1, α_2, allowing only the parameter p to vary.
4. For each trajectory from Step 3, calculate the value of the statistic for all tested τ values.
5. Using the distributions of the statistic values obtained in Steps 2 and 4, compute the empirical Hellinger distance between the distributions of the statistics for FBM and FBMRE in the first scenario, or for SBM and SBMRE in the second scenario. We recall here that if F and Q are two probability measures with probability density functions f and q, respectively, the Hellinger distance between them is defined as follows [42,43]

$$H(F,Q) = \left[\int_{\mathbb{R}} \left(\sqrt{f(x)} - \sqrt{q(x)} \right)^2 dx \right]^{1/2}. \tag{37}$$

As one may observe, the considered statistic is symmetric in its arguments and takes values between 0 and $\sqrt{2}$. A larger value of Hellinger distance indicates a greater separation between the PDFs of the two distributions. The minimum value corresponds to the case where $f(x) = q(x)$ for all x, while the maximum value occurs when $f(x) = 0$ for all non-zero values of $q(x)$, and vice versa. In practice, the theoretical values of $f(x)$ and $q(x)$ are replaced by their estimators, and the so-called empirical Hellinger distance is calculated. In our case, we use the kernel density estimators of the PDFs. It is worth mentioning another distance statistic that can be utilized in this context, namely the Bhattacharyya distance [62]. Both the Bhattacharyya and Hellinger distances are used to measure the similarity or dissimilarity between two probability distributions; however, they differ in their normalization methods and mathematical formulations.
6. Select the τ or τ_1 and τ_2 values that maximize the Hellinger distance between the distributions of the statistic values for the trajectories from anomalous diffusion models with constant parameters (from Step 2) and random parameters (from Step 4).

The results of the procedure described above we present for FBM with $H_0 = \{0.3, 0.4, 0.5, 0.6, 0.7\}$ and FBMRE with $H_1 = 0.2$, $H_2 = 0.8$, and p chosen to ensure that $\mathbb{E}(\mathcal{H}) = H_0$. In the second scenario, we analyze SBM with $\alpha_0 = \{0.6, 0.8, 1, 1.2, 1.4\}$ and SBMRE with $\alpha_1 = 0.4$, $\alpha_2 = 1.6$ and p selected to ensure that $\mathbb{E}(\mathcal{A}) = \alpha_0$. Results are provided for three trajectory lengths: $N = \{100, 500, 1000\}$. For each statistic, $MC = MC^* = 1000$ Monte Carlo simulations were performed (see Steps 1 and 3 of the procedure above). In the

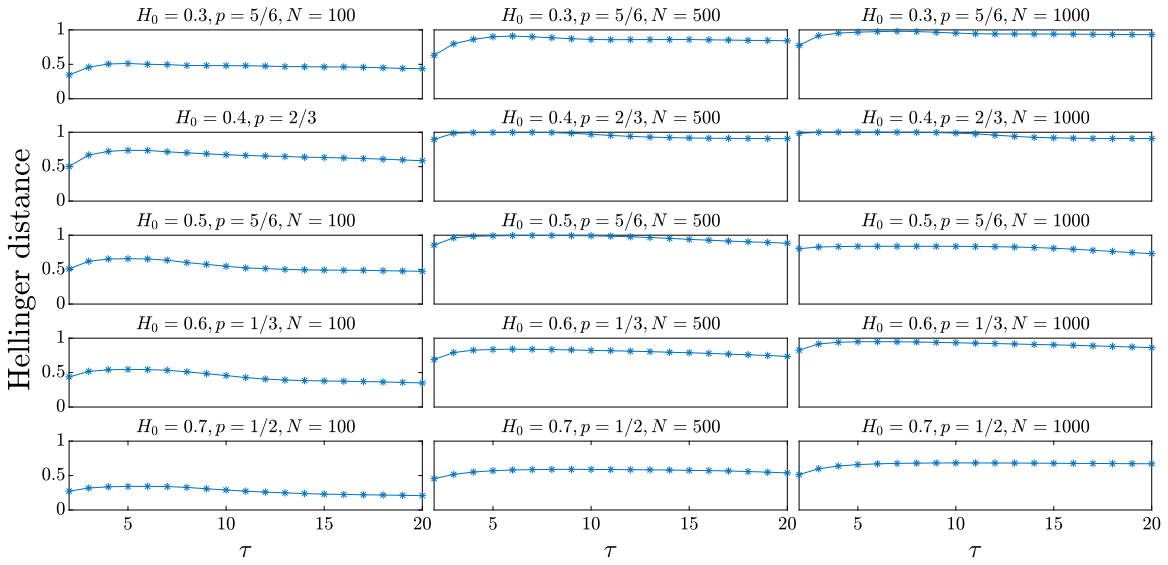

Fig. 3. Hellinger distance between probability distributions of TAMSD statistics for trajectories from FBM with $H_0 = \{0.3, 0.4, 0.5, 0.6, 0.7\}$ and FBMRE with $\mathcal{H} \sim \mathcal{TP}(0.2, 0.8, p)$, where p was chosen to ensure $\mathbb{E}(\mathcal{H}) = H_0$, namely $p = \{5/6, 2/3, 1/2, 1/3, 1/6\}$. Results are presented for three trajectories lengths $N = \{100, 500, 1000\}$. Each row corresponds to a different H_0.

Table 1
Optimal τ, τ_1 and τ_2 selected based on the presented procedure utilizing the Hellinger distance between the distributions of the applied statistics for anomalous diffusion models with constant and random parameters. The analyzed statistics include TAMSD, TAMSD$_R$, EAM, EAM$_R$, DMA, and DMA$_R$. The anomalous diffusion models examined are FBM and SBM (models with constant parameters) and FBMRE and SBMRE (models with random parameters). For the models with random parameters we assume a two-point distribution of the anomalous exponents.

statistic	FBM/FBMRE	SBM/SBMRE
TAMSD	$\tau = 4$	$\tau = 2$
TAMSD$_R$	$\tau_1 = 2, \tau_2 = 10$	$\tau_1 = 3, \tau_2 = 2$
EAM	$\tau = 3$	
EAM$_R$	$\tau_1 = 2, \tau_2 = 20$	
DMA	$\tau = 6$	$\tau = 4$
DMA$_R$	$\tau_1 = 3, \tau_2 = 2$	$\tau_1 = 3, \tau_2 = 2$

first scenario (FBM versus FBMRE), we analyze the statistics TAMSD, TAMSD$_R$, EAM, EAM$_R$, DMA and DMA$_R$. For distinguishing between SBM and SBMRE, we examine only the distributions of TAMSD, TAMSD$_R$, DMA and DMA$_R$.

Sample results are shown in Fig. 3 for TAMSD and in Fig. 4 for TAMSD$_R$, both illustrating the case of FBM versus FBMRE. Based on these plots, we selected the τ values that maximized the Hellinger distance, approaching 1. It is worth mentioning that we cannot use a single set of parameters for all cases. Therefore, we selected the values of τ that yield the highest Hellinger distances in the majority of cases. Additionally, as shown in Figs. 3 and 4, we prioritized the initial τ values that produced good results (similar outcomes were observed across many τ values). In our example, this corresponds to $\tau = 4$ for the TAMSD statistic and $\tau_1 = 2$ and $\tau_2 = 10$ for the TAMSD$_R$ statistic. A similar analysis was conducted for the other statistics considered and for the second scenario. The final results (the selected optimal τ values) for both scenarios – FBM versus FBMRE and SBM versus SBMRE – are presented in Table 1.

5. Simulation study

In this section, we evaluate the efficiency of the procedure proposed in Section 4, which differentiates between anomalous diffusion models with constant and random parameters. As described above, the procedure is based on a testing methodology where the null hypothesis considers FBM, here with $H_0 = \{0.2, 0.3, 0.7, 0.8\}$, and SBM, here with $\alpha_0 = \{0.4, 0.6, 1.4, 1.6\}$. The acceptance regions (see Eq. (36)) for all test statistics – TAMSD, TAMSD$_R$, EAM, EAM$_R$, DMA, DMA$_R$ for the first scenario and TAMSD, TAMSD$_R$, DMA, DMA$_R$ for the second scenario – are calculated using $MC = 1000$ simulated trajectories from the models under the null hypothesis. In the first scenario, the alternative hypothesis is FBMRE with $\mathcal{H} \sim \mathcal{TP}(0.2, 0.8, p)$, while in the second scenario - SBMRE with $\mathcal{A} \sim \mathcal{TP}(0.4, 1.6, p)$, where $p = \{0, 1/6, 2/6, 3/6, 4/6, 5/6, 1\}$ in both cases. Results are based on 1000 trajectories simulated under the alternative hypothesis, showing the percentage of rejected trajectories for each of the tests discussed. In the conducted

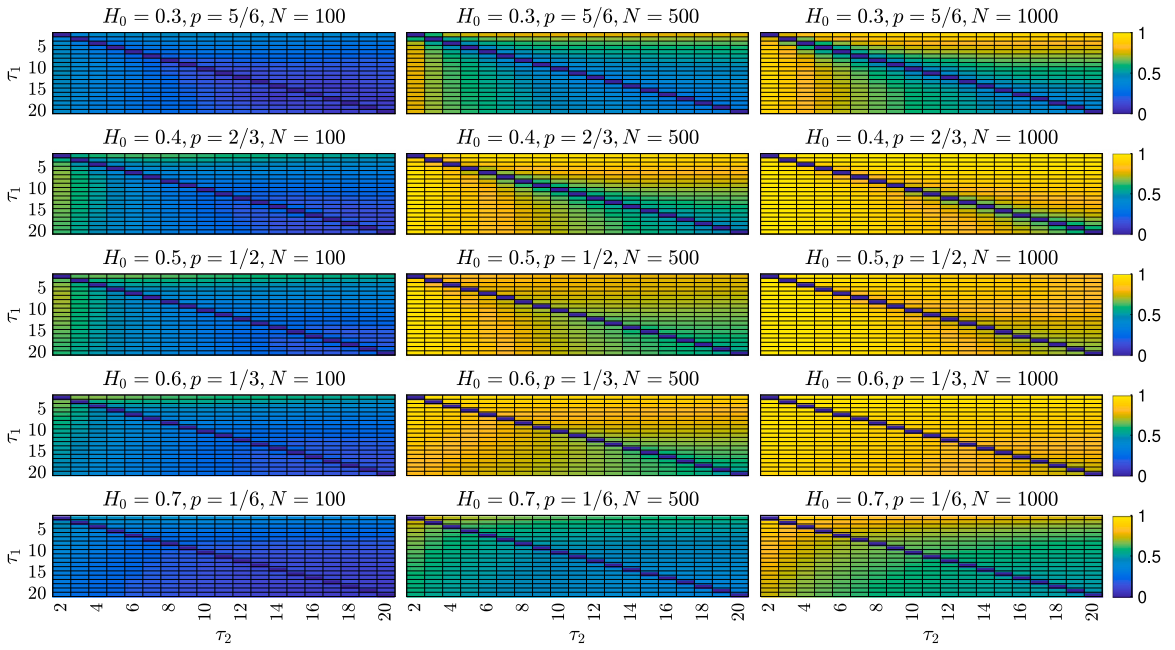

Fig. 4. Hellinger distance between probability distributions of TAMSD_R statistics for trajectories from FBM with $H_0 = \{0.3, 0.4, 0.5, 0.6, 0.7\}$ and FBMRE with $\mathcal{H} \sim \mathcal{TP}(0.2, 0.8, p)$, where p was chosen to ensure $\mathbb{E}(\mathcal{H}) = H_0$, namely $p = \{5/6, 2/3, 1/2, 1/3, 1/6\}$. Results are presented for three trajectories lengths $N = \{100, 500, 1000\}$. Each row corresponds to a different H_0.

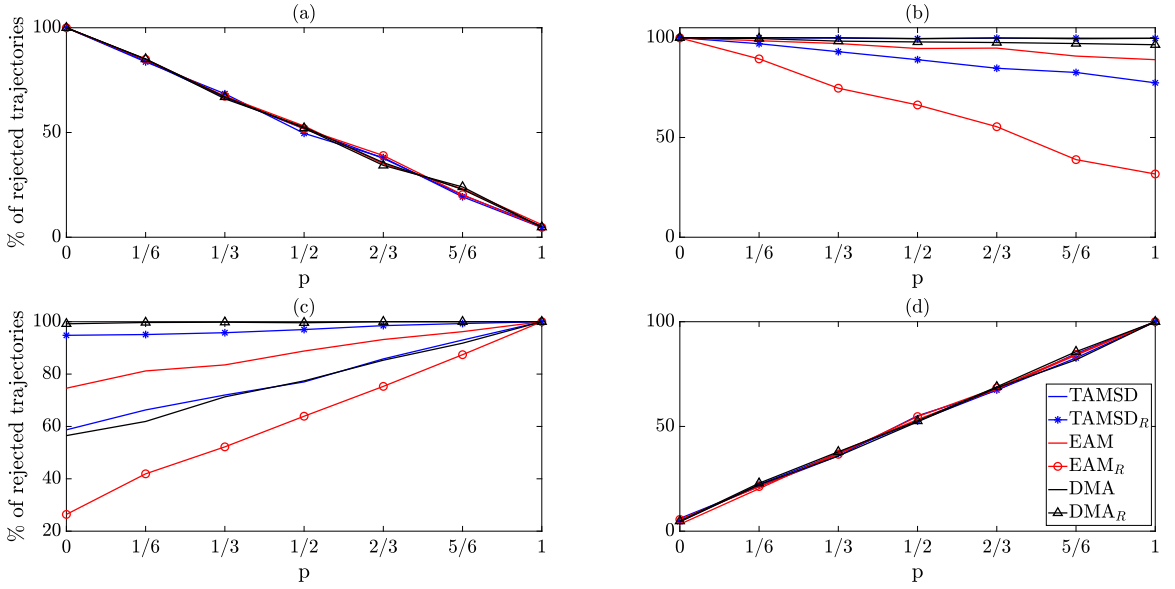

Fig. 5. Percentage of rejected trajectories from the time-averaged statistics-based test, verifying the null hypothesis of FBM against the alternative hypothesis of FBMRE with $\mathcal{H} \sim \mathcal{TP}(0.2, 0.8, p)$. The parameter p varies between 0 and 1. The values of H_0 in the null hypothesis are as follows (a) $H_0 = 0.2$, (b) $H_0 = 0.3$, (c) $H_0 = 0.7$ and (d) $H_0 = 0.8$. The results are based on 1000 simulations of trajectories with length $N = 1000$. For each statistic, the optimal τ is chosen according to the methodology presented in Section 4.1.

simulations, the significance level is set to $c = 0.05$ with the trajectory length of $N = 1000$. In the testing procedure, we use the optimal τ values selected according to the procedure presented in Section 4.1.

In Fig. 5, the results for the first scenario (FBM versus FBMRE) are presented. In Fig. 5(a), the null hypothesis is $H_0 = 0.2$. In this case, when $p = 0$, the two-point distribution reduces to the Dirac delta in point $H_2 = 0.8$, causing the tested FBMRE reducing to FBM with $H_2 = 0.8$, which is consistent with 100% rejection of the null hypothesis of FBM with $H_0 = 0.2$. Conversely, for $p = 1$, the FBMRE in the alternative hypothesis reduces to FBM with $H_1 = 0.2$, and approximately 5% of trajectories are rejected while testing

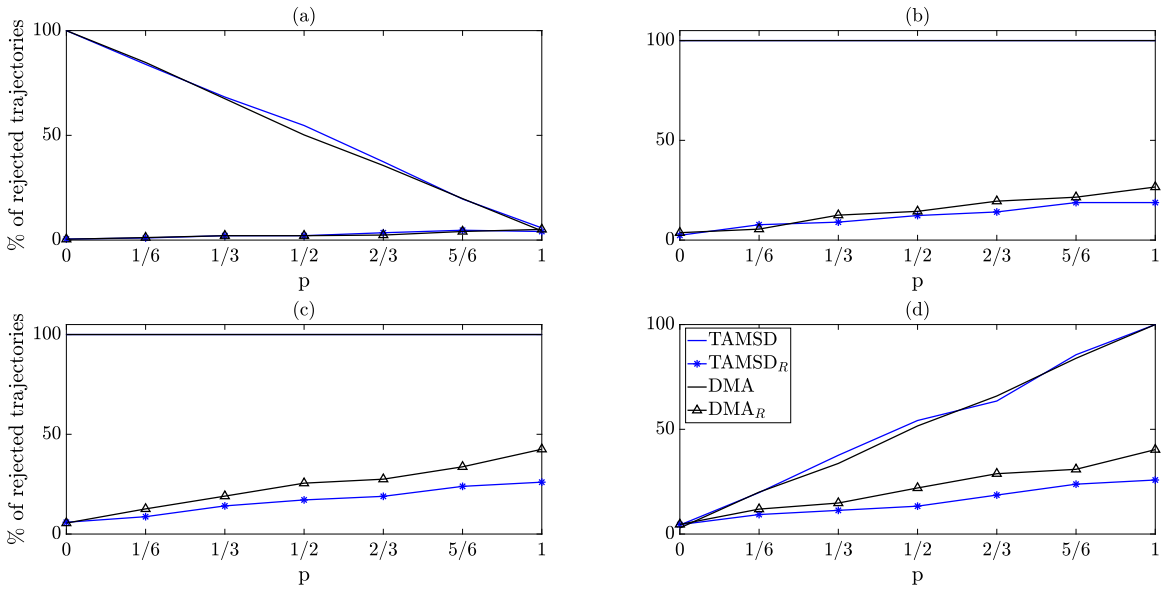

Fig. 6. Percentage of rejected trajectories from the time-averaged statistics-based test, verifying the null hypothesis of SBM against the alternative hypothesis of SBMRE with $\mathcal{A} \sim \mathcal{TP}(0.4, 1.6, p)$. The parameter p varies between 0 and 1. The values of α_0 in the null hypothesis are as follows (a) $\alpha_0 = 0.4$, (b) $\alpha_0 = 0.6$, (c) $\alpha_0 = 1.4$ and (d) $\alpha_0 = 1.6$. The results are based on 1000 simulations of trajectories with lengths $N = 1000$. For each statistic, the optimal τ is chosen according to the methodology presented in Section 4.1.

$H_0 = 0.2$, which is also consistent with the tests' significance level. Thus, all tests perform as expected. In Fig. 5(b), the situation differs slightly. Here, with $H_0 = 0.3$, the two-point distribution never matches the H value specified in the null hypothesis. We observe that the tests based on the EAM$_R$ and TAMSD$_R$ statistics performs the least effectively with smallest rejection rates across all values of p. For TAMSD, DMA, and DMA$_R$, the null hypothesis is nearly always rejected, as expected. In Fig. 5(c), we present results for $H_0 = 0.7$. In this case, the tests based on the EAM$_R$, DMA and TAMSD statistics perform the least effectively. Finally, in Fig. 5(d), we observe the opposite situation compared to Fig. 5(a): the null hypothesis is always rejected for $p = 1$, while for $p = 0$, for approximately 5% of trajectories we do not reject the null hypothesis is not rejected, consistent with the significance level of the tests. Here, the case of $p = 0$ corresponds to FBMRE reducing to FBM with $H_2 = 0.8$ (which aligns with the null hypothesis), while for $p = 1$ FBMRE reduces to FBM with $H_1 = 0.2$, causing 100% rejection rate.

Fig. 6 presents the results for the second scenario, where we evaluate SBMRE trajectories under the null hypothesis that they originate from SBM. In this analysis, we focus on tests based on the TAMSD, TAMSD$_R$, DMA, and DMA$_R$ statistics. Across all panels, it is evident that the tests relying on ratio statistics perform poorly. Specifically, they consistently start near zero from $p = 0$ and increase up to 5% as $p = 1$ for the null hypotheses in Fig. 6(a) or 20% to 40% for the null hypotheses considered in other panels, even though the alternative processes do not align with the one specified in the null hypotheses. In contrast, the tests based on classical statistics, specifically TAMSD and DMA, demonstrate strong performance. As can be noted, when the null hypothesis is set at $\alpha_0 = 0.4$ (Fig. 6(a)) and $p = 0$, these tests reject the null hypothesis, as the SBMRE in the alternative reduces to SBM with $\alpha_0 = 1.6$. Moreover, for $p = 1$, the results align with the 5% significance level, as the SBMRE reduces to the process considered in the null hypothesis. An opposite situation is observed when $\alpha_0 = 1.6$ (Fig. 6(d)): for $p = 0$ the rejection rate is 5%, while for $p = 1$ we observe 100% rejection rate, as expected. In the intermediate cases – Figs. 6(b) and 6(c) – the tests based on classical statistics consistently reject the null hypothesis with the rejection percentage equal to 100% for all values of p.

The results presented above indicate that the effectiveness of the procedure described in Section 4 varies notably depending on the chosen statistics and the specific scenarios. In particular, in the second scenario, we observe a substantial drop in the performance of the ratio statistic-based procedure. While the ratio statistics underperform compared to their classical metric-based counterparts in the first scenario, they are still reasonably effective. However, in the SBM versus SBMRE scenario, they should not be recommended due to their markedly lower reliability. This variation in performance highlights the importance of selecting the most appropriate statistic based on the characteristics of the processes tested, as well as the specific properties of the anomalous exponent distribution.

In Appendix B, we present the results for testing FBM versus FBMRE and SBM versus SBMRE for trajectories that are shorter than $N = 1000$ discussed above. In the first scenario, the results are shown in Fig. B.13 (for $N = 100$) and Fig. B.14 (for $N = 500$), while in the second scenario, they are presented in Fig. B.15 (for $N = 100$) and Fig. B.16 (for $N = 500$). For each statistic, the optimal τ is selected according to the methodology outlined in Section 4.1.

When testing SBM vs. SBMRE, we do not observe significant differences in the efficiency of the testing procedure for shorter trajectories compared to $N = 1000$. The percentage of rejected trajectories remains similar across all considered values of N in corresponding cases. As with $N = 1000$, for $N = 500$ and $N = 100$, the ratio-based statistics underperform compared to their classical counterparts. The latter exhibit similar values of the examined measure, indicating no substantial differences in their performance.

When testing FBM vs. FBMRE, trajectory length generally has a greater impact on the efficiency of the procedure. However, the observed differences in rejection rates for $N = 100$, $N = 500$, and $N = 1000$ depend on the experimental conditions, including the choice of statistic, the tested H_0, and the parameter p. Specifically, when testing $H_0 = 0.2$ or $H_0 = 0.8$, the rejection rates for shorter trajectories are very similar to those observed for $N = 1000$, except for the test based on the EAM_R statistic. Notably, for this statistic, at $N = 100$, a significant decline in performance is observed for all considered values of H_0, but particularly in the case of superdiffusive testing. In this case, the test fails to differentiate between processes for any value of p, with rejection rates close to 0%. This is because the acceptance region defined in Eq. (36) is significantly larger compared to the case with longer trajectories, resulting in the test statistic's value almost always falling within the acceptance region. We observe that EAM statistics performs less efficient for short trajectories, as it is an extension of the sample ACVF, which also exhibits limitations in such cases. The ratio of EAM statistics increases the inefficiency for short trajectories.

In other cases, such as testing $H_0 = 0.3$ or $H_0 = 0.8$, reducing the trajectory length leads to a decrease in rejection rates, making it more difficult to distinguish between processes. Moreover, the choice of the most effective statistic varies depending on the trajectory length. For instance, when testing $H_0 = 0.7$, the highest rejection rate for $N = 1000$ is achieved by DMA_R and TAMSD_R, while for $N = 500$ TAMSD_R remains the best-performing statistic, however, DMA_R is outperformed by EAM. In contrast, for $N = 100$, DMA_R and TAMSD_R are again the most effective, although the differences between all statistics become much less pronounced.

The conducted experiments confirm the importance of selecting the most appropriate testing procedure while also considering trajectory length.

6. Application to real datasets

This section elucidates the practical application of our methodology using two real-world datasets from distinct domains. In the first case we analyze trajectories describing the motion of polystyrene beads in agarose hydrogels, while the second dataset is a time series representing the daily closing prices of Bitcoin (BTC) in USD. Both datasets have been previously analyzed in the literature, where the FBM model was proposed for their characterization. Our analysis confirms that the financial data (BTC) aligns with the classical anomalous diffusion model, whereas the biological data (motion of polystyrene beads) correspond to the FBMRE case.

6.1. Motion of polystyrene beads

The first dataset studies the motion of polystyrene microspheres within agarose hydrogels. The trajectories of individual 50-nm polystyrene beads loaded into a 1.5% agarose gel were recorded [44]. The viscoelastic properties of the agarose gel led to anomalous diffusion of the type of fractional Brownian motion [63]. A 1.5% agarose gel was prepared from agarose powder by dissolving it in phosphate-buffered saline. Polystyrene microspheres with 50-nm diameter (Bangs Laboratories, Fishers, IN) were first heated to 60 ° C in 0.5% Tween 20 and introduced into the agarose solution. The solution was kept at 60 ° C for 15 min and then allowed to slowly cool down. The microspheres were imaged in an inverted microscope with a 40x objective and a scientific CMOS camera at 71 frames/s [44,64]. A total of 2049 images were recorded. The motion of 20 microspheres was tracked in two dimensions in LABVIEW using a cross-correlation-based tracking algorithm [65].

The same dataset was analyzed in [31], where the EAM statistic was utilized to confirm the FBM. In this paper, we extend these results by also applying other time-averaged statistics. Additionally, in our analysis the optimal τ parameters are used, while in [31] we apply the EAM-based methodology for all $\tau \in \{2, 3, \dots, 2049\}$. The final conclusion was based on the fact that for most (90%) of the τ values, the FBM hypothesis was not rejected.

The dataset contains 20 trajectories, each of length $N = 2049$. The analysis is performed on the data corresponding to the X coordinate. In Fig. 7, we show a sample trajectory. First, all trajectories are normalized by the estimated diffusion coefficient obtained using the TAMSD-approach [22]. Then, the methodology presented in Section 4 is applied, where TAMSD, TAMSD_R, EAM, EAM_R, DMA, and DMA_R statistics are used (with the optimal τ values). To construct the acceptance region given in Eq. (36), we generate $MC = 500$ simulated trajectories of FBM with the given $H_0 \in \{0.1, 0.11, 0.22, \dots, 0.89, 0.9\}$, and each trajectory consisting of 2049 observations. Finally, for each H_0 we calculate the percentage of the rejected trajectories, i.e. percentage of trajectories not classified as FBM. The results are presented in Fig. 8(a). Based on these results, we observe that only the approach based on the EAM_R statistic does not reject the null hypothesis for H_0 values close to 0.5 for all of the trajectories. Additionally, we can see that the shapes of the functions presented in Fig. 8(a) correspond to the inverted PDF of two- mode distribution, which indicates that H is not constant. Thus, there is a basis for considering FBMRE as the model for the examined trajectories. As the justification for the conclusion about the randomness of the Hurst exponent, in Fig. 9 we present the compression of the empirical PDF of estimated H corresponding to X coordinate (estimated by TAMSD-approach) with the empirical PDF of 20 values simulated from two-point distribution with parameters obtained from the real trajectories. The empirical PDF is obtained based on the kernel density estimator [66]. To estimate the two-point distribution parameters, we use the following approach. We select H_1 and H_2 (see Eq. (6)) as the modes from the empirical PDF of H estimated from analyzed trajectories. In our case $H_1 = 0.28$ and $H_2 = 0.47$. The corresponding p value is a percentage of trajectories for which the estimated H corresponds to H_1 (i.e. for which the estimated H is smaller than the local minima of the empirical PDF). In our case $p = 1/10$. As can be seen, the PDFs presented in Fig. 9 coincide. Thus, we can assume that the real trajectories originate from the FBMRE with H drawn from a bimodal distribution and the two-point distribution of H can be considered as a simple approximation.

Finally, to confirm the two-point distribution of the anomalous exponent, we simulate 20 trajectories from the FBMRE model (with 2049 points), assuming a two-point distribution of H with parameters estimated from the real trajectories. For such data, we

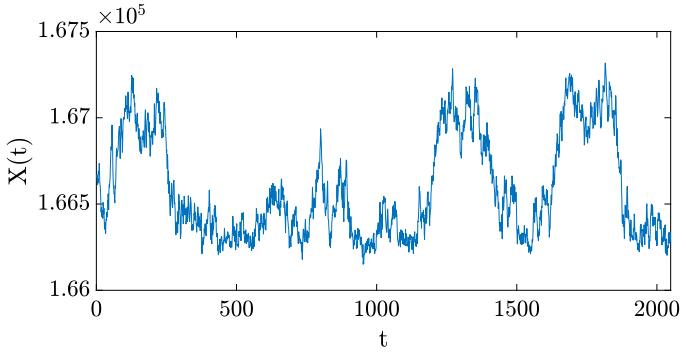

Fig. 7. Sample trajectory of X coordinate.

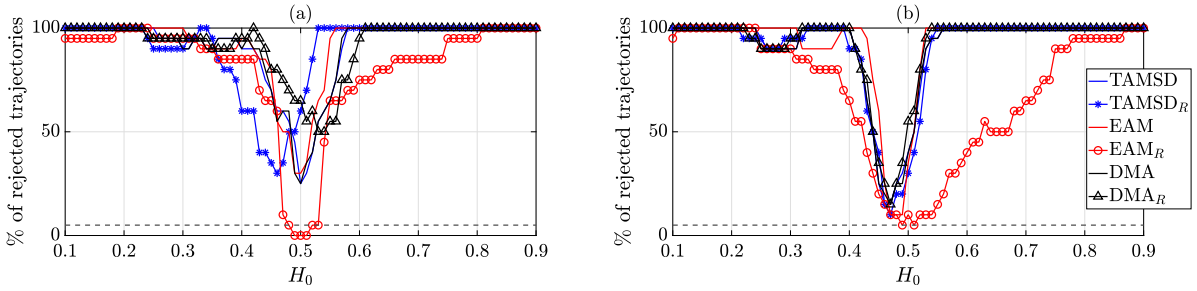

Fig. 8. Motion of polystyrene beads: percent of trajectories not identified as FBM with given H_0 (a). Simulated trajectories from FBMRE with $\mathcal{H} \sim \mathcal{TP}(0.28, 0.47, 1/10)$: percent of trajectories not identified as FBM with given H_0 (b).

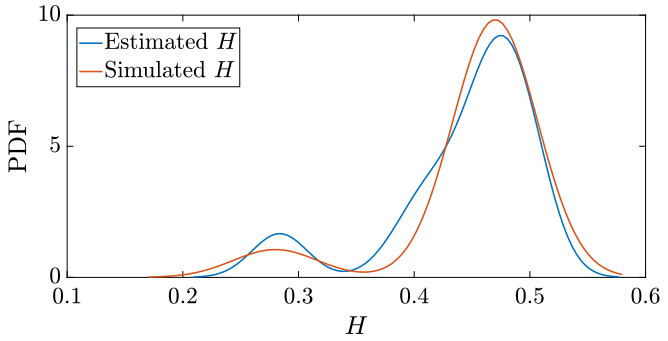

Fig. 9. Comparison of empirical PDF for H estimated from real trajectories using the TAMSD-based approach (blue line) and empirical PDF from H simulated from $\mathcal{TP}(0.28, 0.47, 1/10)$ (red line).

repeat the procedure presented in Section 4 and verify the percentage of trajectories for which the FBM with a given H_0 is rejected. The results are presented in Fig. 8(b). As can be seen, the shapes of the curves presented in the Figs. 8(a) and 8(b) correspond to one another. Similarly to the real trajectories, only the EAM$_R$-based approach does not reject the null hypothesis of FBM for H_0 values close to 0.5 for all trajectories. The motion in agarose hydrogels often exhibits anomalous diffusion due to the viscoelastic nature of the gel [44]. However, hydrogels can have marked heterogeneities that lead to more complex processes such as the ones studied here [67]. In addition, it has been observed that at longer times the motion in agarose hydrogels can cross over to normal diffusion [68]. Therefore, assessing the homogeneity of the medium is an important tool in understanding this complex system.

6.2. Bitcoin time series

In this section, we examine the daily closing prices of BTC collected from October 1, 2013, to March 20, 2021, comprising a total of 2713 samples. Notably, the Bitcoin data were modeled using geometric fractional Brownian motion (gFBM) as described in the referenced article [45]. Let us mention that also scaled geometric Brownian motion (SgBM) can be considered as a potential model for describing Bitcoin prices, as demonstrated in the following paper [69]. In the analysis, we consider the natural logarithm

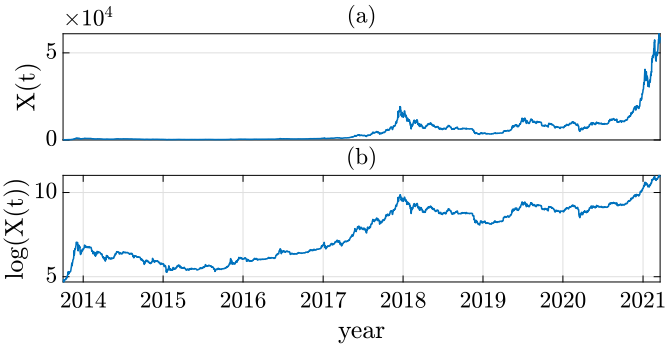

Fig. 10. Daily closing price of Bitcoin (in USD) collected from 1 October 2013 to 20 March 2021, 2713 samples (a). Transformed data (b).

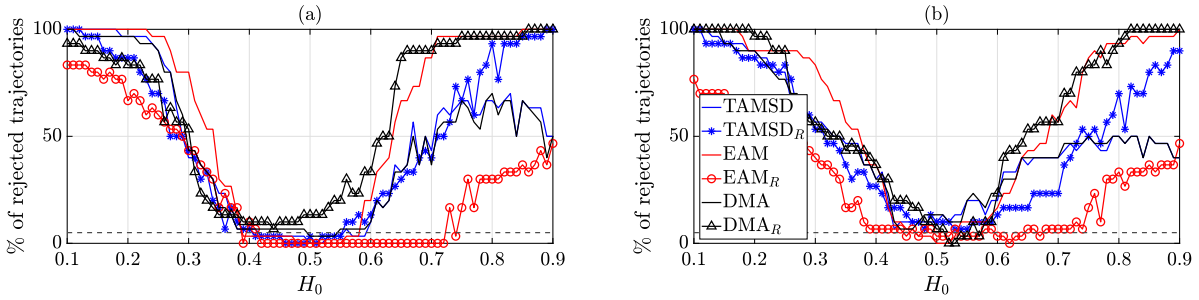

Fig. 11. Bitcoin time series: percent of sub-series not identified as FBM with given H_0 (a). Simulated trajectories from BM: percent of trajectories not identified as FBM with given H_0 (b).

of the raw time series, see Fig. 10(a): raw data; Fig. 10(b): transformed data. To differentiate between models with constant and random parameters, we divided the time series into 30 sub-series, each of length 90 points. The trajectories were then normalized using the estimated diffusion coefficient obtained via the TAMSD-based approach. The same time series was examined in [40], where the authors concluded that the normalized logarithmic closing prices of BTC exhibit FBM-like behavior. In their analysis, the EAM-based procedure was applied, and the corresponding anomalous exponent was found to be close to 0.5. Thus, the analyzed data, in fact, demonstrate behavior consistent with Brownian motion. Our goal is to confirm this hypothesis by applying additional statistics discussed in the current article and by performing analogous procedures for SBM. Specifically, in the first scenario, similar as for the trajectories describing motion of polystyrene beads, for each $H_0 \in \{0.1, 0.11, 0.22, \dots, 0.89, 0.9\}$, we perform the testing procedure described in Section 4 using the TAMSD, TAMSD$_R$, EAM, EAM$_R$, DMA, and DMA$_R$ statistics. To construct the acceptance region given in Eq. (36), in each case we generate $MC = 500$ simulated trajectories of FBM with the given H_0, each of length 90 observations. Finally, we calculate the percentage of rejected trajectories, i.e., those that were not classified as FBM. In the second scenario, we perform the procedure for SBM using $\alpha_0 \in \{0.2, 0.21, 0.22, \dots, 1.79, 1.8\}$, utilizing the TAMSD and DMA statistics. Based on simulation results, where the ratio statistics performed poorly for the SBM case, we decided not to include them in the second scenario. In all cases we applied the optimal τ values selected using the methodology discussed in Section 4.1.

The results for the first scenario are presented in Fig. 11(a). As shown, the outcomes suggest that the analyzed data can be described by FBM with a Hurst parameter close to 0.5. In these cases, most of the statistical tests do not reject the null hypothesis for nearly or over 95% of the trajectories (except for the DMA$_R$-based approach, which indicates a percentage above the 5% level for all values of H_0). Based on these results, we suspect that the data may be described by BM (FBM with $H = 0.5$). Therefore, in Fig. 11(b), we present analogous results obtained from 30 simulated BM trajectories, each of length 90. Namely, we repeat the procedure presented in Section 4 for simulated data and verify the percentage of trajectories for which the FBM with a given H_0 is rejected. As observed, the behavior of the statistical approaches is similar to the real data case, including the EAM$_R$-based approach, for which, across a wide range of H_0 values, we observe low rejection rates (close to 5% level). This similarity supports our hypothesis that the Bitcoin sub-series may originate from BM.

In Fig. 12(a), the results from the second scenario are presented. Similar to the first scenario, for more than 95% of trajectories, the null hypothesis is not rejected when testing BM (here corresponding to $\alpha = 1$) for both approaches. This is consistent with the outcomes obtained in the first scenario. In Fig. 12(b), we also present the results for simulated BM trajectories (with the same sample size and the same number of trajectories as in the real data case). As one can see, although the shape is sharper, these results correspond to the results obtained for real data, i.e., the rejection rates are similar for the corresponding values of α_0.

Thus, based on both tested scenarios, our methodology confirms the findings reported in the literature for the same dataset.

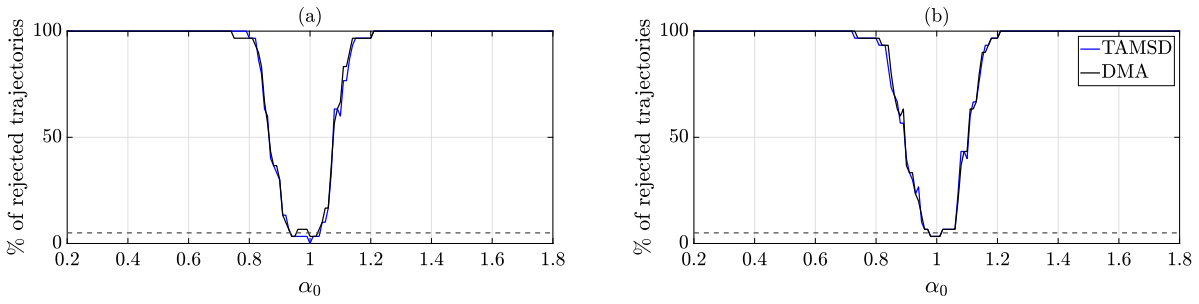

Fig. 12. Bitcoin time series: percent of sub-series not identified as SBM with given α_0 (a). Simulated trajectories from BM: percent of trajectories not identified as SBM with given α_0 (b).

7. Conclusions

In this paper, we address the problem of differentiating between anomalous diffusion models with constant and random parameters. Anomalous diffusion models have been extensively discussed in the literature and have found numerous applications, particularly in describing the motion of particles in single-particle tracking experiments. However, recent experimental evidence suggests that classical models often fail to fully account for observed particle motion behaviors. As a result, modified anomalous diffusion models that capture specific features of the data are increasingly being considered. One such modification involves incorporating random parameters into anomalous diffusion models.

The proposed approach builds on the statistics of time-averages, which are widely used for analyzing classical anomalous diffusion processes (i.e., where parameters are constant). We extend existing methodologies by introducing a relatively simple procedure based on statistical testing, which can be applied to a broad class of processes. As exemplary anomalous diffusion models, we consider FBM and its random exponent variant (FBMRE), as well as SBM and its random exponent variant (SBMRE). We demonstrate the efficacy of the proposed methodology in case where the anomalous exponent follows a two-point distribution.

Our analysis is further supported by real-world data examples, where we examine the motion of polystyrene beads and Bitcoin prices. For the polystyrene beads, our results provide new insights into prior analyses, which identified FBM as the appropriate model for the data. Our findings suggest instead that the data are better described by FBMRE, with an anomalous exponent derived from a two-mode distribution. These data provide a tool for evaluating spatial inhomogeneities in media that can lead to multi-mode distributions. In the case of the hydrogels examined here, we found that the data are better described by a mixture of two Hurst exponents, with most of the trajectories corresponding to a single exponent. For financial data (Bitcoin prices), our results are consistent with findings reported in the literature, confirming Brownian motion as the appropriate model.

Although the presented methodology is discussed in the context of FBM, SBM, and the random anomalous exponent, it can potentially be used to analyze other cases as well, where various mechanisms related to parameter randomness occur. One example is the case of random diffusivity in the anomalous diffusion models discussed, see e.g. [70,71]. The proposed approach could also be applied to processes outside of FBM and SBM, such as confined diffusion described by the Ornstein–Uhlenbeck process, which exhibits linear diffusion at short times and a saturation in TAMSD at long times, see e.g. [72].

We believe that the proposed methodology offers a valuable and versatile tool for practical applications, enabling more precise modeling of anomalous diffusion processes across diverse fields.

Acknowledgments

The work of AW was supported by National Science Centre under Opus Grant 2020/37/B/HS4/00120 “Market risk model identification and validation using novel statistical, probabilistic, and machine learning tools”.

Appendix A. Expected values of time-averaged statistics for FBMRE and SBMRE with two-point distributed anomalous exponent

Fact 4.

1. *Let $\mathbb{X}_n$ denote a trajectory of FBMRE process defined in Section 2.2, where $\mathcal{H}$ follows a two-point distribution with PDF defined in Eq. (6). Then, applying Fact 1, the expected value of the TAMSD is given by the following formula*

$$\mathbb{E}(\mathrm{TAMSD}(\mathbb{X}_n, \tau)) = (1-p)\tau^{2H_1} + p\tau^{2H_2}. \tag{A.1}$$

2. *Let $\mathbb{X}_n$ denote a trajectory of SBMRE process defined in Section 2.4, where $\mathcal{A}$ follows a two-point distribution with PDF defined in Eq. (11). Then, applying Fact 1, the expected value of the TAMSD is given by the following formula*

$$\mathbb{E}(\mathrm{TAMSD}(\mathbb{X}_n, \tau)) = \frac{1}{n-\tau}\sum_{i=1}^{n-\tau}\left((i+\tau)^{H_1}(1-p) + (i+\tau)^{H_2}p - i^{H_1}(1-p) - i^{H_2}p\right). \tag{A.2}$$

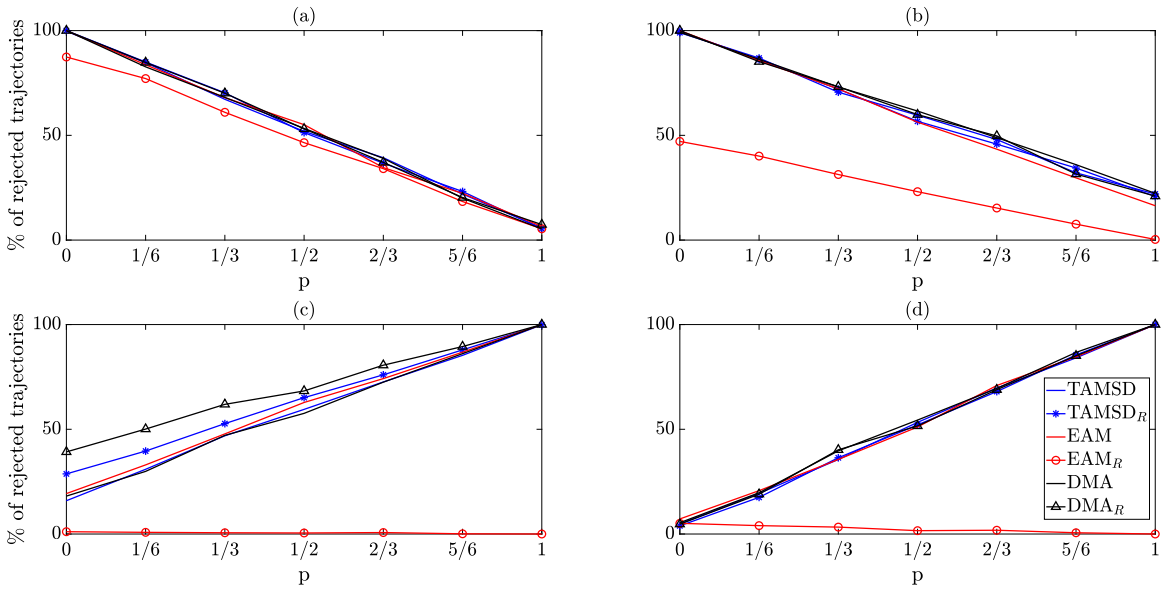

Fig. B.13. Percentage of rejected trajectories from the time-averaged statistics-based test, verifying the null hypothesis of FBM against the alternative hypothesis of FBMRE with $\mathcal{H} \sim \mathcal{TP}(0.2, 0.8, p)$. The parameter p varies between 0 and 1. The values of H_0 in the null hypothesis are as follows (a) $H_0 = 0.2$, (b) $H_0 = 0.3$, (c) $H_0 = 0.7$ and (d) $H_0 = 0.8$. The results are based on 1000 simulations of trajectories with length $N = 100$. For each statistic, the optimal τ is chosen according to the methodology presented in Section 4.1.

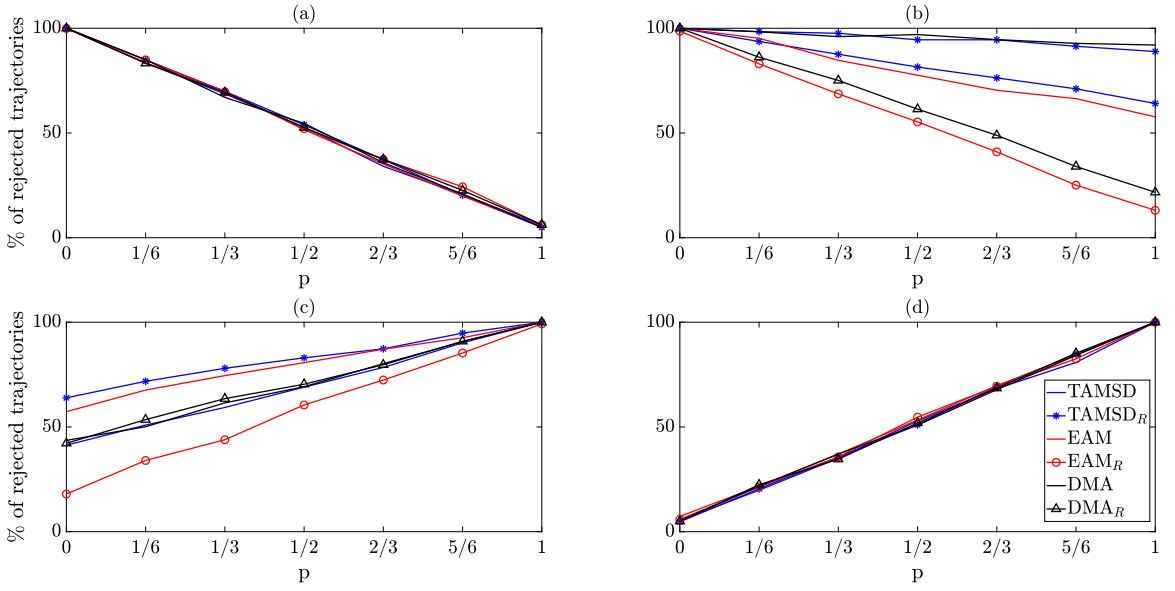

Fig. B.14. Percentage of rejected trajectories from the time-averaged statistics-based test, verifying the null hypothesis of FBM against the alternative hypothesis of FBMRE with $\mathcal{H} \sim \mathcal{TP}(0.2, 0.8, p)$. The parameter p varies between 0 and 1. The values of H_0 in the null hypothesis are as follows (a) $H_0 = 0.2$, (b) $H_0 = 0.3$, (c) $H_0 = 0.7$ and (d) $H_0 = 0.8$. The results are based on 1000 simulations of trajectories with length $N = 500$. For each statistic, the optimal τ is chosen according to the methodology presented in Section 4.1.

Fact 5.

1. *Let $\mathbb{X}_n$ denote a trajectory of FBMRE process defined in Section 2.2, where $\mathcal{H}$ follows a two-point distribution with PDF defined in Eq. (6). Then, applying Fact 2, the expected value of the EAM is given by the following formula*

$$\mathbb{E}(\mathrm{EAM}(\mathbb{X}_n, \tau)) = p\tau^{2H_1} + (1-p)\tau^{2H_2} - \tau. \tag{A.3}$$

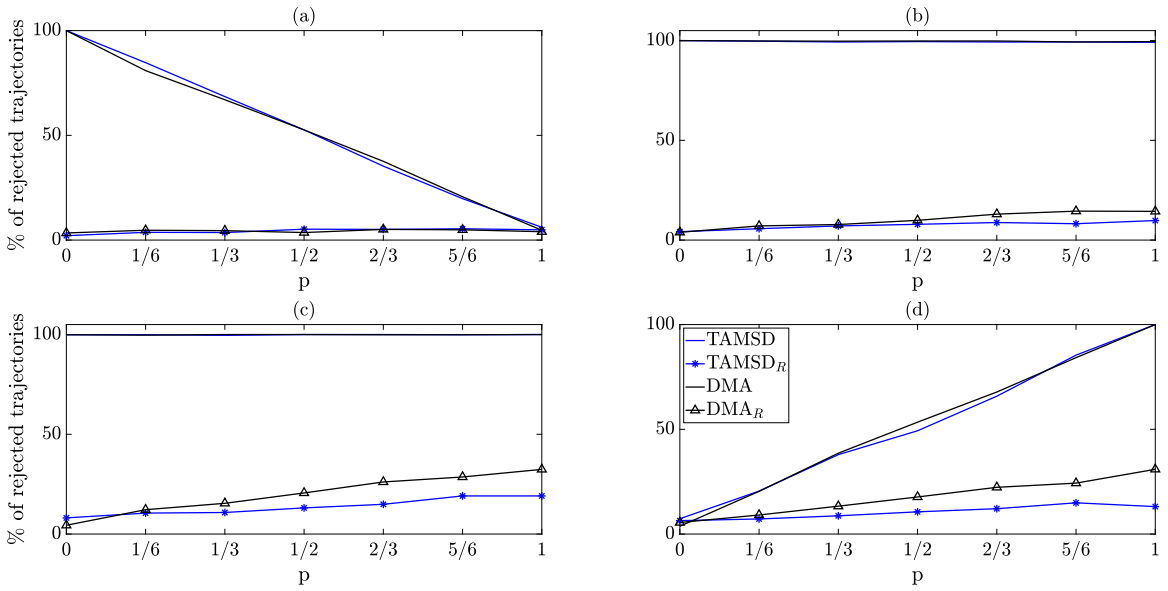

Fig. B.15. Percentage of rejected trajectories from the time-averaged statistics-based test, verifying the null hypothesis of SBM against the alternative hypothesis of SBMRE with $\mathcal{A} \sim \mathcal{TP}(0.4, 1.6, p)$. The parameter p varies between 0 and 1. The values of α_0 in the null hypothesis are as follows (a) $\alpha_0 = 0.4$, (b) $\alpha_0 = 0.6$, (c) $\alpha_0 = 1.4$ and (d) $\alpha_0 = 1.6$. The results are based on 1000 simulations of trajectories with lengths $N = 100$. For each statistic, the optimal τ is chosen according to the methodology presented in Section 4.1.

Fact 6.

1. *Let $\mathbb{X}_n$ denote a trajectory of FBMRE process defined in Section 2.2, where $\mathcal{H}$ follows a two-point distribution with PDF defined in Eq. (6). Then, applying Fact 3, the expected value of the DMA is given by the following formula*

$$\begin{aligned}\mathbb{E}(\mathrm{DMA}(\mathbb{X}_n,\tau)) = \frac{1}{n-\tau}\sum_{j=\tau}^{n}\Bigg\{&\left(1-\frac{1}{\tau}\right)^2\left(j^{2H_1}p + j^{2H_2}(1-p)\right)\\ &+\left(\frac{1}{\tau^2}-\frac{1}{\tau}\right)\sum_{m=j-\tau+1}^{j-1}\left(\left(j^{2H_1}+m^{2H_1}-|j-m|^{2H_1}\right)p+\left(j^{2H_2}+m^{2H_2}-|j-m|^{2H_2}\right)(1-p)\right)\\ &+\frac{1}{\tau^2}\sum_{m=j-\tau+1}^{j-1}\left(m^{2H_1}p+m^{2H_2}(1-p)\right)\\ &+\frac{2}{\tau^2}\sum_{j-\tau+1\le l<m\le j-1}\left(\left(m^{2H_1}+l^{2H_1}-|m-l|^{2H_1}\right)p+\left(m^{2H_2}+l^{2H_2}-|m-l|^{2H_2}\right)(1-p)\right)\Bigg\}.\end{aligned} \tag{A.4}$$

2. *Let $\mathbb{X}_n$ denote a trajectory of SBMRE process defined in Section 2.2, where $\mathcal{A}$ follows a two-point distribution with PDF defined in Eq. (11). Then, applying Fact 3, the expected value of the DMA is given by the following formula*

$$\begin{aligned}\mathbb{E}(\mathrm{DMA}(\mathbb{X}_n,\tau)) = \frac{1}{n-\tau}\sum_{j=\tau}^{n}\Bigg\{&\left(1-\frac{1}{\tau}\right)^2\left(j^{H_1}p + j^{H_2}(1-p)\right)\\ &+2\left(\frac{1}{\tau^2}-\frac{1}{\tau}\right)\sum_{m=j-\tau+1}^{j-1}\left(\min\{j,m\}^{H_1}p+\min\{j,m\}^{H_2}(1-p)\right)+\frac{1}{\tau^2}\sum_{m=j-\tau+1}^{j-1}\left(m^{H_1}p+m^{H_2}(1-p)\right)\\ &+\frac{2}{\tau^2}\sum_{j-\tau+1\le l<m\le j-1}\left(\min\{m,l\}^{H_1}p+\min\{m,l\}^{H_2}(1-p)\right)\Bigg\}.\end{aligned} \tag{A.5}$$

Appendix B. Results for $N = 100$ and $N = 500$

See Figs. B.13–B.16.

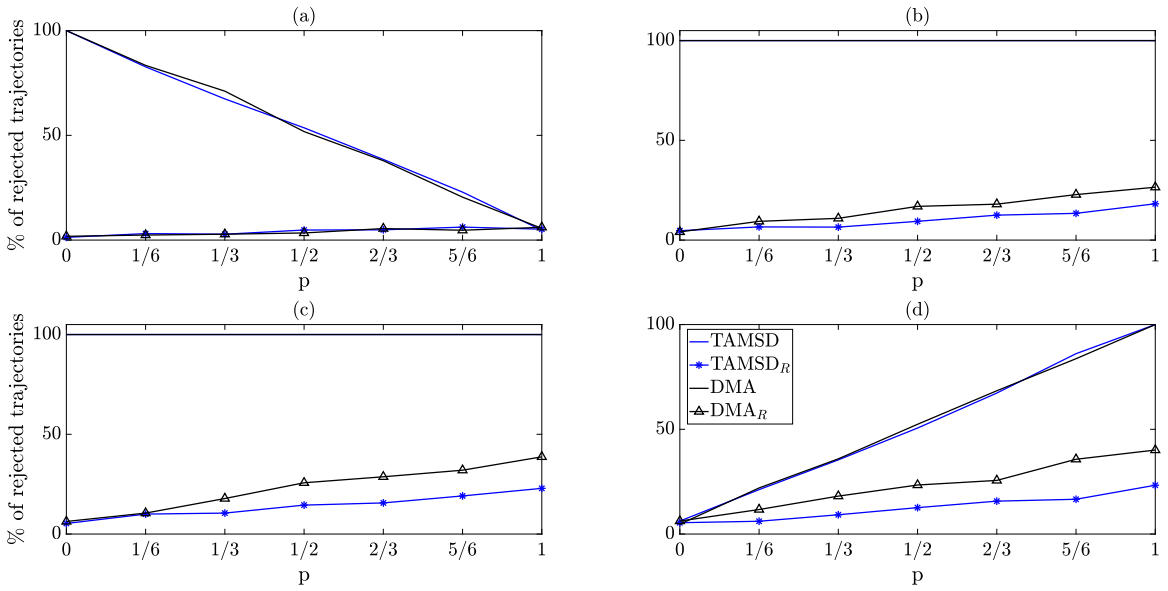

Fig. B.16. Percentage of rejected trajectories from the time-averaged statistics-based test, verifying the null hypothesis of SBM against the alternative hypothesis of SBMRE with $\mathcal{A} \sim \mathcal{TP}(0.4, 1.6, p)$. The parameter p varies between 0 and 1. The values of α_0 in the null hypothesis are as follows (a) $\alpha_0 = 0.4$, (b) $\alpha_0 = 0.6$, (c) $\alpha_0 = 1.4$ and (d) $\alpha_0 = 1.6$. The results are based on 1000 simulations of trajectories with lengths $N = 500$. For each statistic, the optimal τ is chosen according to the methodology presented in Section 4.1.

Data availability

The data that has been used is available upon request.

References

[1] J. Crank, The Mathematics of Diffusion, in: Oxford science publications, Clarendon Press, 1979.
[2] H. Berg, Random Walks in Biology, in: Princeton paperbacks, Princeton University Press, 1993.
[3] A. Fowler, Mathematical Models in the Applied Sciences, in: Cambridge Texts in Applied Mathematics, Cambridge University Press, 1997.
[4] J.L. Schnoor, Environmental Modeling : Fate and Transport of Pollutants In Water, Air, and Soil, Wiley, New York (N.Y.), 1996.
[5] E. Cussler, Diffusion: Mass Transfer in Fluid Systems, in: Cambridge Series in Chemical Engineering, Cambridge University Press, 2009.
[6] A. Einstein, Über die von der molekularkinetischen theorie der Wärme geforderte bewegung von in ruhenden Flüssigkeiten suspendierten Teilchen, Ann. Phys., Lpz. 322 (8) (1905) 549–560.
[7] M. von Smoluchowski, Zur kinetischen theorie der Brownschen molekularbewegung und der suspensionen, Ann. Phys., Lpz. 326 (14) (1906) 756–780.
[8] H. Scher, E.W. Montroll, Anomalous transit-time dispersion in amorphous solids, Phys. Rev. B 12 (1975) 2455–2477.
[9] J.-P. Bouchaud, A. Georges, Anomalous diffusion in disordered media: Statistical mechanisms, models and physical applications, Phys. Rep. 195 (4) (1990) 127–293.
[10] R. Metzler, J. Klafter, The random walk's guide to anomalous diffusion: a fractional dynamics approach, Phys. Rep. 339 (1) (2000) 1–77.
[11] D. Krapf, Chapter five - mechanisms underlying anomalous diffusion in the plasma membrane, in: A.K. Kenworthy (Ed.), Lipid Domains, in: Current Topics in Membranes, vol. 75, Academic Press, 2015, pp. 167–207.
[12] R. Metzler, J.-H. Jeon, A.G. Cherstvy, E. Barkai, Anomalous diffusion models and their properties: non-stationarity, non-ergodicity, and ageing at the centenary of single particle tracking, Phys. Chem. Chem. Phys. 16 (2014) 24128–24164.
[13] V. Sposini, D. Krapf, E. Marinari, R. Sunyer, F. Ritort, F. Taheri, C. Selhuber-Unkel, R. Benelli, M. Weiss, R. Metzler, G. Oshanin, Towards a robust criterion of anomalous diffusion, Commun. Phys. 5 (2022) 305.
[14] A.N. Kolmogorov, Wienersche spiralen und einige andere interessante Kurven in Hilbertscen Raum, C.R.(Doklady), Acad. Sci. URSS (NS) 26 (1940) 115–118.
[15] B.B. Mandelbrot, J.W. Van Ness, Fractional Brownian motions, fractional noises and applications, SIAM Rev. 10 (4) (1968) 422–437.
[16] J. Beran, Statistics for Long-Memory Processes, Chapman & Hall, 1994.
[17] S.C. Lim, S.V. Muniandy, Self-similar Gaussian processes for modeling anomalous diffusion, Phys. Rev. E 66 (2002) 021114.
[18] G.K. Batchelor, Diffusion in a field of homogeneous turbulence: II. The relative motion of particles, Math. Proc. Cambridge Philos. Soc. 48 (2) (1952) 345–362.
[19] M. Magdziarz, A. Weron, Ergodic properties of anomalous diffusion processes, Ann. Physics 326 (9) (2011) 2431–2443.
[20] H. Hassani, N. Leonenko, K. Patterson, The sample autocorrelation function and the detection of long-memory processes, Phys. A 391 (24) (2012) 6367–6379.
[21] A. Sabri, X. Xu, D. Krapf, M. Weiss, Elucidating the origin of heterogeneous anomalous diffusion in the cytoplasm of mammalian cells, Phys. Rev. Lett. 125 (2020) 058101.
[22] G. Sikora, K. Burnecki, A. Wyłomańska, Mean-squared-displacement statistical test for fractional Brownian motion, Phys. Rev. E 95 (2017) 032110.
[23] A.V. Weigel, B. Simon, M.M. Tamkun, D. Krapf, Ergodic and nonergodic processes coexist in the plasma membrane as observed by single-molecule tracking, Proc. Natl. Acad. Sci. 108 (16) (2011) 6438–6443.

[24] O. Vilk, E. Aghion, T. Avgar, C. Beta, O. Nagel, A. Sabri, R. Sarfati, D.K. Schwartz, M. Weiss, D. Krapf, R. Nathan, R. Metzler, M. Assaf, Unravelling the origins of anomalous diffusion: From molecules to migrating storks, Phys. Rev. Res. 4 (2022) 033055.
[25] K. Maraj, D. Szarek, G. Sikora, A. Wyłomańska, Empirical anomaly measure for finite-variance processes, J. Phys. A 54 (2) (2020) 024001.
[26] G. Sikora, Statistical test for fractional Brownian motion based on detrending moving average algorithm, Chaos Solitons Fractals 114 (2018) 54–62.
[27] A.M. Mathai, S.B. Provost, Quadratic forms in random variables: theory and applications, Marcel Dekker, 1992.
[28] O. Vilk, E. Aghion, R. Nathan, S. Toledo, R. Metzler, M. Assaf, Classification of anomalous diffusion in animal movement data using power spectral analysis, J. Phys. A 55 (33) (2022) 334004.
[29] M. Balcerek, K. Burnecki, G. Sikora, A. Wyłomańska, Discriminating Gaussian processes via quadratic form statistics, Chaos:Interdiscip. J. Nonlinear Sci. 31 (6) (2021) 063101.
[30] M. Balcerek, K. Burnecki, Testing of fractional Brownian motion in a noisy environment, Chaos, Solitons & Fractals 140 (2020) 110097.
[31] D. Szarek, K. Maraj-Zygmąt, G. Sikora, D. Krapf, A. Wyłomańska, Statistical test for anomalous diffusion based on empirical anomaly measure for Gaussian processes, Comput. Statist. Data Anal. 168 (2022) 107401.
[32] P. Kowalek, H. Loch-Olszewska, Ł. Łaszczuk, J. Opała, J. Szwabiński, Boosting the performance of anomalous diffusion classifiers with the proper choice of features, J. Phys. A 55 (24) (2022) 244005.
[33] H. Seckler, J. Szwabiński, R. Metzler, Machine-learning solutions for the analysis of single-particle diffusion trajectories, J. Phys. Chem. Lett. 14 (35) (2023) 7910–7923.
[34] A.G. Cherstvy, S. Thapa, C.E. Wagner, R. Metzler, Non-Gaussian, non-ergodic, and non-Fickian diffusion of tracers in mucin hydrogels, Soft Matter 15 (12) (2019) 2526–2551.
[35] K. Speckner, M. Weiss, Single-particle tracking reveals anti-persistent subdiffusion in cell extracts, Entropy 23 (7) (2021) 892.
[36] R. Benelli, M. Weiss, From sub-to superdiffusion: Fractional Brownian motion of membraneless organelles in early C. elegans embryos, New J. Phys. 23 (2021) 063072.
[37] A.A. Sadoon, Y. Wang, Anomalous, non-Gaussian, viscoelastic, and age-dependent dynamics of histonelike nucleoid-structuring proteins in live Escherichia coli, Phys. Rev. E 98 (2018) 042411.
[38] M. Balcerek, K. Burnecki, S. Thapa, A. Wyłomańska, A. Chechkin, Fractional Brownian motion with random hurst exponent: Accelerating diffusion and persistence transitions, Chaos: An Interdiscip. J. Nonlinear Sci. 32 (9) (2022) 093114.
[39] H. Woszczek, A. Chechkin, A. Wyłomańska, Scaled Brownian motion with random anomalous diffusion exponent, Commun. Nonlinear Sci. Numer. Simul. 140 (1) (2025) 108388.
[40] A. Grzesiek, J. Gajda, S. Thapa, A. Wyłomańska, Distinguishing between fractional Brownian motion with random and constant hurst exponent using sample autocovariance-based statistics, Chaos: An Interdiscip. J. Nonlinear Sci. 34 (4) (2024) 043154.
[41] K. Maraj, D. Szarek, G. Sikora, A. Wyłomańska, Time-averaged mean squared displacement ratio test for Gaussian processes with unknown diffusion coefficient, Chaos: An Interdiscip. J. Nonlinear Sci. 31 (7) (2021) 073120.
[42] E. Hellinger, Neue Begrüündung der theorie quadratischer formen von unendlichvielen Verääänderlichen, ournal die Reine und Angewandte Mathematik 136 (1909) 210–271.
[43] G.L. Yang, L.M. Le Cam, Asymptotics in statistics: Some basic concepts, Springer (2020).
[44] D. Krapf, N. Lukat, E. Marinari, R. Metzler, G. Oshanin, C. Selhuber-Unkel, A. Squarcini, L. Stadler, M. Weiss, X. Xu, Spectral content of a single non-Brownian trajectory, Phys. Rev. X 9 (2019) 011019.
[45] M. Tarnopolski, Modeling the price of bitcoin with geometric fractional Brownian motion: a Monte Carlo approach, 2017, arXiv:1707.03746.
[46] B.B. Mandelbrot, J.W. Van Ness, Fractional Brownian motions, fractional noises and applications, SIAM Rev. 10 (4) (1968) 422–437.
[47] S.C. Lim, S.V. Muniandy, Self-similar Gaussian processes for modeling anomalous diffusion, Phys. Rev. E 66 (2002) 021114.
[48] A.G. Cherstvy, W. Wang, R. Metzler, I.M. Sokolov, Inertia triggers nonergodicity of fractional Brownian motion, Phys. Rev. E 104 (2021) 024115, http://dx.doi.org/10.1103/PhysRevE.104.024115.
[49] A. Fuliński, Anomalous diffusion and weak nonergodicity, Phys. Rev. E 83 (2011) 061140, http://dx.doi.org/10.1103/PhysRevE.83.061140.
[50] A. Fuliński, Communication: How to generate and measure anomalous diffusion in simple systems, J. Chem. Phys. 138 (2) (2013) 021101, http://dx.doi.org/10.1063/1.4775737.
[51] A.G. Cherstvy, H. Safdari, R. Metzler, Anomalous diffusion, nonergodicity, and ageing for exponentially and logarithmically time-dependent diffusivity: striking differences for massive versus massless particles, J. Phys. D: Appl. Phys. 54 (19) (2021) 195401, http://dx.doi.org/10.1088/1361-6463/abdff0.
[52] W. Wang, R. Metzler, A.G. Cherstvy, Anomalous diffusion, aging, and nonergodicity of scaled Brownian motion with fractional Gaussian noise: overview of related experimental observations and models, Phys. Chem. Chem. Phys. 24 (2022) 18482–18504, http://dx.doi.org/10.1039/D2CP01741E.
[53] A. Mathai, S. Provost, Quadratic forms in random variables: Theory and applications, J. Amer. Statist. Assoc. 87 (420) (1992) 1244–1245.
[54] E. Kepten, A. Weron, G. Sikora, K. Burnecki, Y. Garini, Guidelines for the fitting of anomalous diffusion mean square displacement graphs from single particle tracking experiments, PLoS One 10 (2) (2015) 1–10.
[55] G. Sikora, M. Teuerle, A. Wyłomańska, D. Grebenkov, Statistical properties of the anomalous scaling exponent estimator based on time-averaged mean-square displacement, Phys. Rev. E 96 (2017) 022132.
[56] X. Michalet, Mean square displacement analysis of single-particle trajectories with localization error: Brownian motion in an isotropic medium, Phys. Rev. E 82 (2010) 041914.
[57] N. Gal, D. Lechtman-Goldstein, D. Weihs, Particle tracking in living cells: a review of the mean square displacement method and beyond, Rheol. Acta 52 (2013) 425–443.
[58] J.-H. Jeon, A.V. Chechkin, R. Metzler, Scaled Brownian motion: a paradoxical process with a time dependent diffusivity for the description of anomalous diffusion, Phys. Chem. Chem. Phys. 16 (2014) 15811–15817.
[59] E. Alessio, A. Carbone, G. Castelli, V. Frappietro, Second-order moving average and scaling of stochastic time series, Eur. Phys. J. B 27 (2002) 197–200.
[60] H. Loch-Olszewska, J. Szwabiński, Impact of feature choice on machine learning classification of fractional anomalous diffusion, Entropy 22 (12) (2020) 1436.
[61] K. Maraj, D. Szarek, G. Sikora, A. Wyłomańska, Time-averaged mean squared displacement ratio test for Gaussian processes with unknown diffusion coefficient, Chaos: An Interdiscip. J. Nonlinear Sci. 31 (7) (2021) 073120.
[62] A. Bhattacharyya, On a measure of divergence between two statistical populations defined by their probability distributions, Bull. Calcutta Math. Soc. 35 (1943) 99–109, 10358.
[63] A.J. Levine, T.C. Lubensky, One- and two-particle microrheology, Phys. Rev. Lett. 85 (2000) 1774–1777.
[64] D. Krapf, E. Marinari, R. Metzler, G. Oshanin, X. Xu, A. Squarcini, Power spectral density of a single Brownian trajectory: what one can and cannot learn from it, New J. Phys. 20 (2018).
[65] C. Gosse, V. Croquette, Magnetic tweezers: micromanipulation and force measurement at the molecular level, Biophys. J. 82 (2002).
[66] Z. Botev, J. Grotowski, D. Kroese, Kernel density estimation via diffusion, Ann. Statist. 38 (2010) 2916–2957.
[67] M.T. Valentine, P.D. Kaplan, D. Thota, J.C. Crocker, T. Gisler, R.K. Prud'homme, M. Beck, D.A. Weitz, Investigating the microenvironments of inhomogeneous soft materials with multiple particle tracking, Phys. Rev. E 64 (2001) 061506.
[68] D.S. Banks, C. Tressler, R.D. Peters, F. Höfling, C. Fradin, Characterizing anomalous diffusion in crowded polymer solutions and gels over five decades in time with variable-lengthscale fluorescence correlation spectroscopy, Soft Matter 12 (2016) 4190–4203.

[69] A.G. Cherstvy, D. Vinod, E. Aghion, I.M. Sokolov, R. Metzler, Scaled geometric Brownian motion features sub- or superexponential ensemble-averaged, but linear time-averaged mean-squared displacements, Phys. Rev. E 103 (2021) 062127, http://dx.doi.org/10.1103/PhysRevE.103.062127.
[70] W. Wang, F. Seno, I.M. Sokolov, A.V. Chechkin, R. Metzler, Unexpected crossovers in correlated random-diffusivity processes, New J. Phys. 22 (2020) 083041.
[71] A. Maćkała, M. Magdziarz, Statistical analysis of superstatistical fractional Brownian motion and applications, Phys. Rev. E 99 (2019) 012143.
[72] T. Uneyama, T. Miyaguchi, T. Akimoto, Relaxation functions of the Ornstein-Uhlenbeck process with fluctuating diffusivity, Phys. Rev. E 99 (2019) 032127.